Journal of Building Engineering 111 (2025) 113352

Contents lists available at ScienceDirect

Journal of Building Engineering

journal homepage: www.elsevier.com/locate/jobe

Prediction of natural carbonation depths in concretes with ensemble metamodel based on artificial neural networks from time series analysis with 20 years of exposure

Tiago Ferreira Campos Neto [a], Oswaldo Cascudo [b,*]

[a] School of Civil and Environmental Engineering, PPG-GECON, Federal University of Goiás (UFG), Goiânia, GO, 74690-900, Brazil
[b] School of Civil and Environmental Engineering, PPG-GECON, Federal University of Goiás (UFG), Brazil

ARTICLE INFO

Keywords:
Concrete structures
Carbonation
Service life
Artificial neural networks
Time series analysis

ABSTRACT

Considering the growing use of carbonation depth prediction models based on artificial neural networks, the ensemble architecture stands out due to its ability to combine different predictive models into a single metamodel, increasing the accuracy of predictions. However, applying these cybernetic models requires greater rigor on the completeness and robustness of the databases employed in the training and validation phases of neural networks. Treating the carbonation depth databases as time series can be a favorable strategy to guarantee completeness and robustness. Thus, this article aims to predict the carbonation depths of concrete structures using an AVR-SARIMA-LSTM-MLP ensemble metamodel with hybrid architecture for neural networks associated with time series analysis. The metamodel was based on several individual SARIMA-LSTM-MLP predictor models trained and validated with information from 36 concretes with different water/binder ratios (0.40, 0.55, and 0.77), types of mineral additions (rice husk ash, fly ash, blast furnace slag, metakaolin, silica fume, and reference – no mineral addition), and curing conditions (wet and dry). The concrete database was made available by the GEDur group and has 2313 depths of natural carbonation measured over 20 years of exposure in a controlled environment. The results of the AVR-SARIMA-LSTM-MLP ensemble metamodel predicted values for about 67 years after the concrete was produced, recording an average correlation coefficient of 0.93 and RMSE between 0.05 and 4.69 mm. These results demonstrate that the ensemble predictor metamodel has high predictive capacity, excellent precision, and accuracy, regardless of the characteristics and properties of the concretes, curing, and exposure conditions.

1. Introduction

The increased exposure time and consequent aging of concrete structures indicate the importance of predicting their useful life to ensure compliance with the minimum service and safety requirements for their users. Implementing strategies to monitor and predict the progress of negative appearances in a structural system is essential to ensure that preventive maintenance, such as inspection and repair, is properly performed, reducing impacts and costs with corrective work.

The carbonation of concrete structures is a pathological manifestation originating from the reaction of carbon dioxide (CO_2) with hydrates – mainly calcium hydroxide ($Ca(OH)_2$) – in the cementitious matrix that may compromise their useful life. The alkaline

* Corresponding author.
E-mail address: ocascudo@ufg.br (O. Cascudo).

https://doi.org/10.1016/j.jobe.2025.113352
Received 9 December 2024; Received in revised form 24 June 2025; Accepted 28 June 2025
Available online 1 July 2025

products from the hydration of the cement are consumed in the carbonation reactions, decreasing the pH of the pore solution. As a result, when the phenomenon advances beyond the concrete cover and reaches the reinforcements, the chemical stability of the passivation film of the steel surface is affected, and corrosion can manifest in the presence of oxygen and moisture. Once initiated, corrosion results in the expansion of the reinforcement volume, causing cracks in the concrete cover and rapid deterioration of the structure [1–3].

In the initial periods, carbonation is more accelerated and its rate tends to reduce as the advancement of this phenomenon modifies the microstructure of the hardened cement slurry. The CO_2 diffusion rate in the lowest concentration layers of the concrete will depend on the porosity of the hydrated slurry and the amount of water available for dissolution. However, the advancement of carbonation reduces the total porosity – due to the precipitation of calcium carbonate – and a decrease in the alkaline reserve, which results in the deceleration of the phenomenon over time. Campos Neto [4] analyzed the pattern of carbonation curves (depth versus exposure time) of concretes with different compositions, types of mineral additives, and curing conditions subjected to natural carbonation for 20 years. Through time series analysis (TSA) techniques, three distinct stages of the curves were identified, as illustrated in Fig. 1.

Basically, the stages differ by the trends, curve slopes, and variability of the values: *i)* Stage I refers to the initial period, which is the first four years, where carbonation occurs in an accelerated manner due to favorable conditions for this phenomenon; *ii)* Stage II encompasses the fifth and tenth (or twelfth depending on the characteristics and properties of the concretes) years present lower variations than the first stage, characterizing the deceleration of the advancement of the carbonation fronts and, finally; *iii)* Stage III, after the tenth (or twelfth) year, has a static character, i.e., the carbonation depths tend to stabilize and not present statistically significant variations.

For future predictions, regardless of the phenomenon studied, the details of the past must be understood. For a more absolute approach, validating the prediction based on a portion of past data is not enough; rather, to visualize the phenomenon from a global perspective, understanding its evolution from the beginning is required to establish the evolutionary pattern. Both carbonation and factors that affect its behavior, such as the exposure conditions and the degree of hydration of the cement, are time-dependent and vary through the years.

The carbonation fronts can be influenced by numerous factors, divided into two groups (Fig. 2): *i)* internal, associated with the

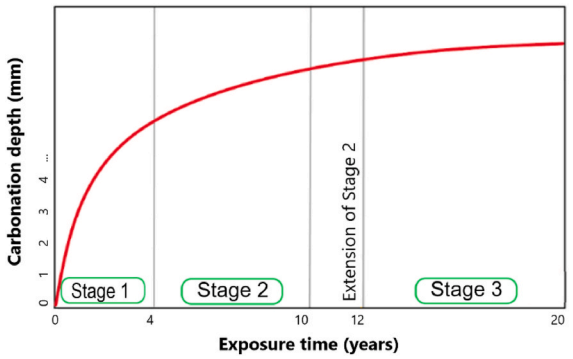

Fig. 1. Representative curve of the carbonation of concrete identifying the temporal periods of the stages over 20 years of exposure to natural carbonation [4]. It should be noted that the curve is a schematic representation of the typical progression of carbonation over time, as observed in various experimental studies with different types of binders. Works such as Youn [1], Cascudo and Carasek [2], and Medeiros, Andrade and Helene [3] show the same qualitative behavior characterized by different stages.

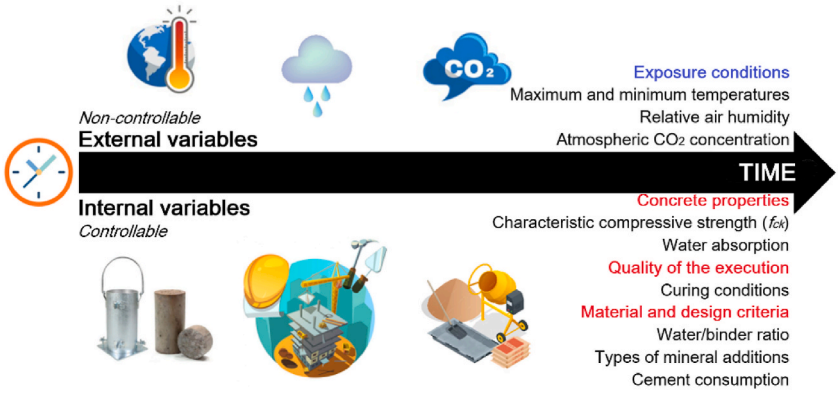

Fig. 2. Factors/variables that influence the carbonation of concretes considered in this study as input signals of predictive models based on neural networks.

controllable variables inherent to the concrete (specifically the pore system and alkaline reserve), for example, material composition [5], design criteria [6], quality of the execution [7], and concrete properties [8]; and *ii)* external, associated with the non-controllable variables inherent to the exposure conditions [9,10] and time of the structures [6,8]. Controllable variables can be modified according to the needs and quality specifications of the concretes guaranteed by professionals [11]. All variables act simultaneously on the concretes; therefore, the synergistic effect on carbonation must be considered.

Concretes with high w/b ratios [6], mineral additions and low cement consumption [12], no or inadequate curing [9], and low compressive strength and high water absorption [13] tend to show accelerated evolution of carbonation. In this same perspective, high atmospheric concentrations of CO_2 [14], high air temperatures [15], and relative humidity between 50 % and 80 % favor the acceleration of carbonation.

The service life of concrete structures can be predicted based on different approaches, including accelerated tests and deterministic and stochastic models. Numerous models have already been proposed [16–25], all based on the estimation of the carbonation front and the mathematical model of Tuutti [26]. This model, whose roots are in Fick's First Law of Diffusion, stands out for its simplicity and accuracy, integrating the effects of all factors that influence carbonation into a single coefficient. This model is effective, especially in structures with more than ten years of exposure to natural carbonation. A large volume of research uses the model as a starting point for new propositions, which mostly focus on investigating the coefficient. The studies have focused on understanding the significance of the effects of the various factors on the phenomenon and its relationships.

In this context, prediction models based on artificial neural networks (ANN) have been satisfactorily applied, as they can capture the synergistic effect of factors on concrete carbonation. The neural networks proved capable of capturing complex interactions between environmental and physicochemical variables, allowing synergistic effects to be modeled, such as the interaction between humidity and CO_2 concentration, which simultaneously affect the progress of carbonation [27–31].

Several studies [32–46] highlight the efficiency of ANN in predicting carbonation, whose coefficients of determination are usually greater than 0.90 and errors less than 14 %. Some studies compared the performance of several algorithms, such as backpropagation (BP), Levenberg-Marquardt, Random Forest, Decision Trees, Support Vector Machine, and Particle Swarm Optimization, but the best performer was not identified. All studies indicate BP as a great algorithm option for predicting carbonation fronts. For ANN topology, the Multilayer Perceptron (MLP) is implemented most; however, this considers fixed input signals, limiting the complexity of the prediction.

Recent advances in machine learning modeling for material prediction tasks, such as those by Tang et al. [47], Yakub et al. [48], and Biala [49] have demonstrated the growing use of neural networks and hybrid models in engineering contexts. Compared to those works, the present study uniquely combines statistical and neural modeling to improve temporal resolution in long-term carbonation prediction. In addition, among the alternative topologies, Long Short-Term Memory (LSTM) – isolated or hybrid – has been applied in the predictions of carbonation fronts [50–63], recording mean square errors (MSE) in the order of 0.40 mm^2. LSTM is indicated to deal with complex problems in time series (TSs), as they have associative memories and can decide on the storage of past information to predict future data.

Among the most recent and robust types, predictive models based on ensemble learning networks have been discussed and applied in recent years. This architecture developed in the 1990s allows aggregate predictions from a group of predictive neural networks in a single metamodel. The group of predictors is called an ensemble, and its results are superior to those of individual (isolated) models, as it generates responses based on crowd knowledge. Thus, even if one of the predictor ANNs does not present satisfactory results, the grouped metamodel may be able to make good predictions, provided that some predictors with adequate results [64,65]. Taffese and Sistonen [66] developed ensemble models to determine the significant parameters controlling concrete chloride ion access using long-term field data. The models were trained using data with the variables that describe the component materials in the concretes, the properties in the fresh and hardened states, the exposure conditions, and the chloride profiles. As a result, models based on grouping by averages could determine the optimal subset of variables that best predicts the chloride profile from the input data.

For carbonation, when considering exposure conditions as input of ANNs, the studies adopt fixed average values independent of the exposure time, which does not represent the actual climatic/environmental conditions to which concretes are subjected. These climatic and environmental variables exhibit seasonality and trends through the years, and adopting average values to feed the predictor models can produce biased results that are not consistent with future reality. This indicates the importance of considering the association of other techniques that allow data to be treated as time series, i.e., inserted into the predictor models to consider their seasonality and trend in the predictions.

Therefore, understanding the evolutionary pattern of carbonation over time and predicting its future behavior are very relevant in the spectrum of the durability of concrete structures. Thus, this article aims to predict carbonation depths based on an AVR-SARIMA-LSTM-MLP ensemble metamodel employing artificial neural networks with hybrid architecture associated with time series analyses. For this, a database of 36 concretes with different compositions, types of mineral additions, and curing conditions was used, made available by the Concrete Durability Study Group (GEDur), and subjected to natural carbonation for 20 years.

2. Materials and methods

Fig. 3 is a flowchart of the steps and tasks developed in this study. Steps 1, 2, 4, and 5 encompass the study and treatment activities of the databases, while steps 3 and 6 are the implementation activities of the artificial neural networks. To better understand the methodology, this section is divided into three major parts.

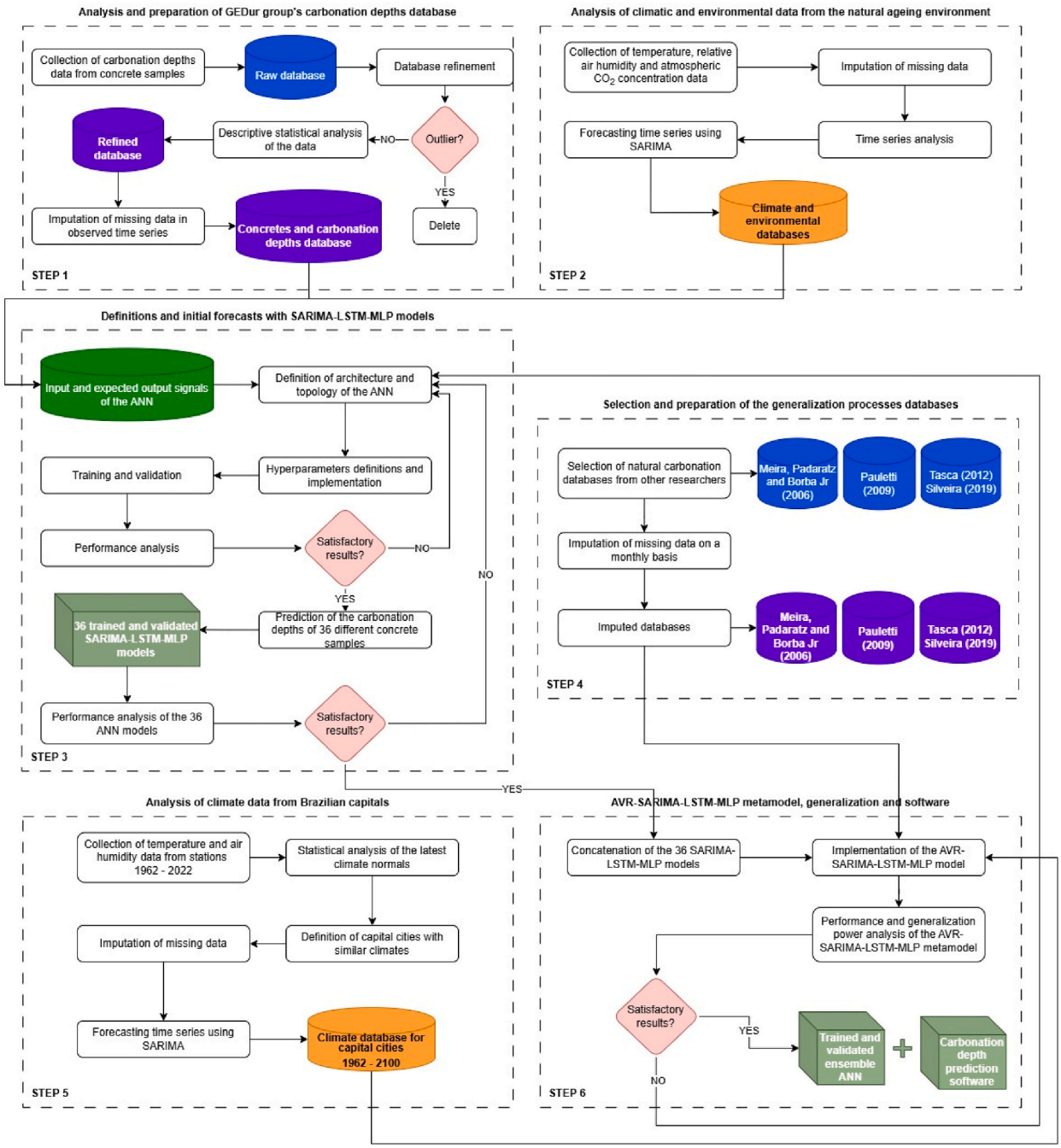

Fig. 3. Flowchart of stages of this study. Six distinct steps of employing databases and implementing predictive models based on artificial neural networks are presented.

-Study and prepare the GEDur group database: The presentation, refinement, and statistical analysis of the carbonation depths database of the 36 concretes were explored.

- **The time series analyses (TSAs) of climate and environmental data:** The TSAs of climate and environmental data over 20 years and predictions were employed in the predictor models based on ANNs.
- **Implement predictor models based on artificial neural networks:** Definitions were made on individual and ensemble predictor models, from the training to validation of the results of concrete carbonation front predictions.

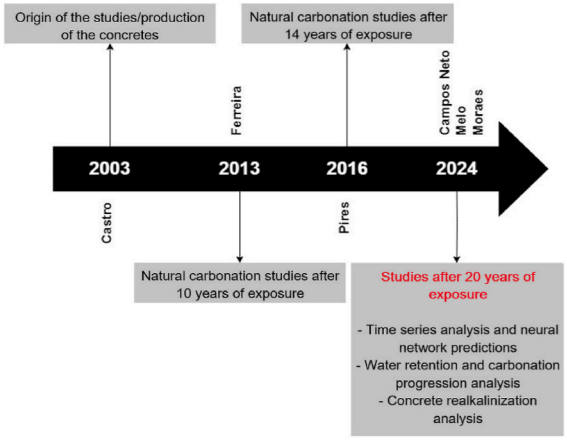

Fig. 4. History of the main research developed by the GEDur group using the natural carbonation database of concrete over 20 years.

2.1. Study and preparation of the GEDur group database

This section presents the activities related to step 1 of Fig. 3.

The database used to develop this study was produced and monitored by GEDur, a partnership between the Federal University of Goiás, Furnas Centrais Elétricas, and the National Electric Energy Agency (ANEEL). This collection of 20 years of natural carbonation data of concrete produced by Castro [67] in 2002 has been studied by several researchers, according to the history of the main research developed by the group illustrated in Fig. 4.

The database was maintained and monitored by the same research team over the 20-year period, with periodic measurements conducted in a controlled environment at the Furnas Centrais Elétricas facilities. The testing procedures were standardized from the beginning of the research, using calibrated instruments, repeated measurements to verify accuracy, and systematic documentation of all steps. These measures ensured traceability and mitigated systematic and random errors over time.

The concretes produced included various mechanical, physical, and chemical properties, resulting in different natural carbonations. The main parameters, including water/binder ratio (w/b), types of mineral additions, and curing conditions, were determined as follows:

- **w/b ratio**: 0.40, 0.55, and 0.70.
- **Type of mineral addition (abbreviation – content)**: blast furnace slag (BFS – 65 %), silica fume (SF – 10 %), metakaolin (M – 10 %), fly ash (FA – 25 %), rice husk ash (RHA – 10 %), and reference (R – 0 %). The contents were established by partially replacing bulk Portland cement.
- **Concrete curing condition**: wet (28 days of curing in a humidity chamber with a temperature of 23 ± 2 °C and air humidity greater than 90 %) and dry (without performing curing procedures).

These variations resulted in 36 different concretes (also called samples) totaling 108 prototypes of reinforced concrete beams with dimensions of 20 × 20 × 50 cm (Fig. 5a). The beams were reinforced with four longitudinal reinforcing bars with a nominal diameter of

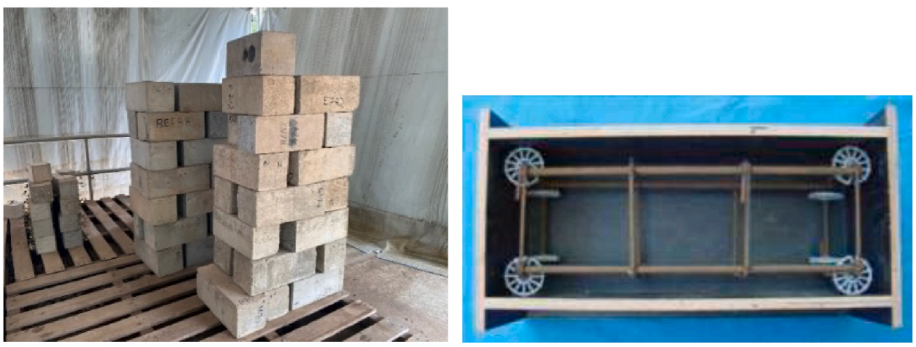

(a) (b)

Fig. 5. Controlled storage/aging environment of concrete beam prototypes for natural carbonation depth tests over 20 years of exposure (a) and plywood forms for molding the specimens (b).

10 mm and stirrups of 5 mm, ensuring a concrete cover of 25 mm (Fig. 5b), according to the environmental aggressiveness class for the storage environment established in the NBR 6118 [68]. The prototypes were designed to replicate the characteristics of real concrete structural components, considering the presence of reinforcement and the use of 12 mm thick resin plywood forms for molding. Because they were stacked, the prototypes were moved every six months to ensure that all faces were subjected to the same exposure conditions. It is important to highlight, throughout the study, that no faces of the concrete prototypes were identified as being preferentially carbonated in relation to others, and that the carbonation fronts appeared reasonably uniform.

During the 20 years of exposure, 2313 individual carbonation depths of the beam prototypes were collected at irregular intervals: 0.75, 3, 7, 9, 10, 14, and 20 years. For each concrete, about 65 measurements of carbonation fronts were performed, i.e., between six and eight measurements per sample/age. The robustness of this bank has worldwide relevance for the technical collections associated with natural carbonation studies. In addition to its expressiveness, it is unique, and the same research group continuously monitored and measured samples under the same exposure conditions.

The storage/aging environment is located in the city of Aparecida de Goiânia, GO, at the Furnas Centrais Elétricas facilities, which is in the Brazilian climate zone called Tropical Central Brazil. The exposure conditions monitored – throughout 2023 – include temperature, relative humidity, and atmospheric CO_2 concentration. According to values recorded by the IP-2000C datalogger – duly calibrated – all climatic and environmental variables were equivalent to those recorded by the Brazilian National Institute of Meteorology (INMET) [69] in the city of Goiânia, GO (code 83423). The values recorded are characteristic of urban heat islands, i.e., the concrete samples were arranged in an environment equivalent to an urban zone, with annual temperatures between 15 and 34 °C, relative humidity between 35 % and 74 %, and CO_2 concentrations between 550 and 750 ppm.

The atmospheric CO_2 concentrations were compared to those available from the Mauna Loa Observatory controlled by the National Oceanic and Atmospheric Administration (NOAA) [70] of the United States Department of Commerce. The correlation coefficient between the values was 0.50; however, the values registered by NOAA are in line with those presented in the literature [22,23]. We therefore opted to adopt the values collected from NOAA. This strategy seeks to increase the accuracy of predictions of carbonation fronts with ANN-predictor models, avoiding the insertion of fixed average values that represented the 20 years of exposure to natural carbonation.

Due to the extensive results of this study, we chose to present the results of seven samples (Table 1), randomly selected from among the 36 (Table A.1 – Appendix A), ensuring that all levels adopted for each variable were considered. Table A.1 also presents the values of cement consumption, characteristic compressive strength (f_{ck}), and water absorption through immersion.

The database was refined by analyzing outliers separated by sample and age of data collection. The flow of activities began with the investigation of possible suspicious values through normal distribution analyses and box plots, followed by the uni- and bilateral Dixon and Grubbs tests [71]. Subsequently, temporal coherence analyses were performed of data evolution and k nearest neighbors (kNN) tests.

Finally, as the depth time series for carbonation of the concretes did not present regular intervals between the observations, a deterministic prediction model of high reliability was used to simulate the real scenario to determine the best technique for imputation of missing data. The selected model was proposed by Tuutti [26] and is among the most reliable in the literature, either due to its ease of application or high precision, especially in concretes with more than 10 years of exposure to natural carbonation [22,23,72–75]. The study by Campos Neto and Cascudo [76] contains the results of the analysis of the techniques to impute missing data in the carbonation time series of the GEDur group database. For sequential data of carbonation depths, the most indicated imputation technique is cubic monotonic spline interpolation. The results of this study include the adjustment and final formatting of the TSs of the natural carbonation depths of the 36 concretes over the 20 years of exposure.

Table 1
Cutting of the concrete samples selected to present the results of this study. The list with all samples and complementary information is presented in Table A.1 of Appendix A.

Samples	w/b ratio	Curing condition	Mineral addition	Alternative identification (abbreviation considering the type of addition, the w/b ratio and the curing condition)
1	0.40 (4)	Wet (W)	Reference (R)	R4W
11	0.55 (5)		Metakaolin (M)	M5W
15	0.70 (7)		Fly ash (FA)	FA7W
16	0.40 (4)		Rice husk ash (RHA)	RHA4W
19	0.40 (4)	Dry (D)	Reference (R)	R4D
24	0.70 (7)		Blast furnace slag (BFS)	BFS7D
26	0.55 (5)		Silica fume (SF)	SF5D

Table 2
Classification of the performance index (*c*) according to Camargo and Sentelhas [81].

Performance index (*c*)	Performance class
>0.85	Excellent
0.76 a 0.85	Very good
0.66 a 0.75	Good
0.61 a 0.65	Average
0.51 a 0.60	Sufferable
0.41 a 0.50	Poor
≤0.40	Bad

2.2. Time series analyses of climate and environmental data

This section presents the tasks related to steps 2 and 5 of Fig. 3.

In addition to the data for the carbonation depths, data collected from the Goiânia weather station (maximum and minimum temperatures and relative humidity) and the Mauna Loa Observatory (atmospheric CO_2 concentration) were also analyzed from the perspective of the TSAs. The following statistical analyses were conducted:

- **Imputation of missing data:** This task consisted of imputing missing data from the TSs of maximum and minimum temperatures and air humidity using the linear interpolation technique with monthly timestamps. The CO_2 concentration data did not need to be imputed since NOAA [70] provides the properly processed information. The imputations were made in the data recorded between January 01, 1962 and 31/12/2022, considering two climatic norms. It is important to describe that 732 monthly temperature and humidity data were collected from INMET [69]. Only 15 of the 732 data points were missing and, for this reason, linear interpolation was chosen.
- **Time series analysis**: A major concern about the quality of data for concrete exposure conditions when predicting with ANN models is based on the ability of the model to capture climate change and understand its effects on carbonation. With this in mind, the TSAs of the climate data were done with the same granularity as the carbonation series, with a monthly timestamp. The climatic and environmental TSs were submitted to the Seasonal-Trend Decomposition using Loess Smoothing techniques to identify trend, seasonality, and residuals over time; Autocorrelation and Partial Autocorrelation functions to identify and quantify the correlation between observations with different time delays; the Mann-Kendall test associated with the Theil-Sen to evaluate the average rate of change of the values over time, quantifying the trend; and the Kruskal-Wallis test to detect possible cycles and variations of the data in different periods. The time frame for the TSAs was limited to the observations during the period equivalent to the exposure of the concrete samples, i.e., between April 2002 and March 2022, constituting 20 years of exposure.
- **Time series prediction**: Among all the variables considered in this study, only climatic and environmental variables display variations over the years. Therefore, it was necessary to predict future values so that these data could be inserted as input signals in the predictor models based on ANNs. The Seasonal Autoregressive Integrated Moving Average (SARIMA) was adopted with orders (p, d, q) (P, D, Q) S, as it stands out for its high accuracy in climate time series predictions [77,78]. Orders were determined using the Akaike information criterion (AIC), whose function is to balance the quality of the fit with the complexity of the SARIMA model. To interpret and validate the predictions, the future scenarios defined in the AR6 report prepared by the Intergovernmental Panel on Climate Change (IPCC) [79] were considered. For the predictions, each climate and environmental time series was composed of 732 monthly observations (including data from 1962 to 2022), and the predictions were made, taking 80 % of the data for training, 10 % for validation, and 10 % for testing the SARIMA predictor models.
- **Analysis and preparation of climate data from Brazilian capitals**: To generalize the knowledge of predictive models based on ANNs, climate data from several Brazilian capitals were properly prepared and predicted. The databases of maximum and minimum temperatures and relative humidity were extracted from INMET [69], including two climatic normals (from 1962 to 2022). These data underwent imputation of missing data and time series prediction. In summary, the process followed the same steps performed for the Goiânia weather station database.
- **Performance analysis**: To determine the performance of the results, criteria such as root mean square error (RMSE), agreement index (d) by Willmott et al. [80], Pearson's correlation coefficient (R), and performance index (*c*) by Camargo and Sentelhas [81] were evaluated. The *c* index can be classified according to Table 2.

2.3. Implementation of predictive models based on artificial neural networks

This section presents the tasks related to steps 3, 4, and 6 of Fig. 3.

The implementation activities of the ANN-predictor models followed the phases of construction, training, validation, generalization, and evaluation of the quality of the predictions. Initially, as established in step 3, predictive models were developed for each of the 36 concretes of the GeEDur group, i.e., 36 ANNs were built with the same architecture, topology, and hyperparameters but with different input and output signals (expected responses/labels). After the validation of the 36 individual predictor models, a single ensemble predictor metamodel resulting from the grouping of the individual models was developed, as described in step 6. This metamodel, with the same architecture as the individual ones, was properly trained and validated and then submitted to evaluations of

knowledge generalization power, considering the results of steps 4 and 5 as new input and output signals. The strategy of implementing an ensemble metamodel with 36 individual predictor models assumes that allowing parameters to be automatically adjusted based on multiple signals improves the generalizability and performance of the metamodel [82,83].

2.3.1. Individual predictor models

This section presents the tasks related to step 3 of Fig. 3.

One of the first tasks for implementing the individual predictor models was defining the input and output signals. In this study, the signals include the information from the GEDur group database divided into three groups: *i)* internal input signals: parameters associated with the characteristics and properties of the concretes, such as w/b ratio, type of mineral addition, curing condition, cement consumption, f_{ck}, and water absorption by immersion; *ii)* external input signals: parameters associated with the age and exposure conditions of the concretes, including exposure time, maximum and minimum temperatures, relative air humidity, and atmospheric CO_2 concentration; and *iii*) output signals: natural carbonation depths of the concretes over the 20 years of exposure. All input and output signals for training of predictor models and their respective levels are illustrated in Fig. 2 and detailed in Table 3.

For the proper functioning of the individual predictor models, the data were properly normalized by applying the Z-score technique to avoid the input and output signals presenting very discrepant magnitudes, and the neurons functioned in the saturation region, which could affect performance during training. For the selected topologies, we decided to apply a hybrid ANN of LSTM and MLP. The choice of this combination stems from the ability of LSTM networks to capture long-term temporal dependencies in time series, while MLPs are effective at modeling nonlinear relationships between variables. This synergy allows the model to handle complex and heterogeneous sequential data, such as that from prolonged natural exposure.

According to Liu, Zhao, and Huang [84], this hybrid system performs well in modeling complex temporal sequences, as LSTM can effectively identify long-term temporal dependencies due to the existence of associative memory cells, whereas MLP can be used for complex and nonlinear characteristics of the data. In this LSTM-MLP hybrid model, the data are processed sequentially, i.e., the input signals continue to be entered even after the validation period. Thus, for external input signals – unlike most studies that fix exposure conditions in terms of fixed averages – their seasonality and trends over time were considered, applying the predicted results from the SARIMA models as input signals. Therefore, using climate and environmental data predicted by other statistical models as part of the input signals, individual ANN-based predictor models for carbonation fronts are considered SARIMA-LSTM-MLP hybrids.

The semi-supervised character of machine learning should be noted, as the SARIMA-LSTM-MLP models seek to find a relationship between the pairs of input and output signals provided for the first 20 years and, after this period, the unlabeled data is employed to

Table 3
Input and output signals considering the variables and their respective levels for training and validation of individual models.

Input and output signals	Variables	Levels
Internal input signals	w/b ratio	0.40 0.55 0.70
	Curing conditions	Wet (28 days) Dry (no curing)
	Mineral additions (partial cement replacement content in mass)	Reference (no mineral addition) Blast furnace slag (65 %) Silica fume (10 %) Metakaolin (10 %) Fly ash (25 %) Rice husk ash (10 %)
	Cement consumption (kg/m^3)[a]	95.90 to 552.0 (12 levels)
	f_{ck} (MPa)[a]	15.0 to 40.0 (6 levels)
	Water absorption (%)[a]	3.16 to 6.04 (18 levels)
External input signals	Exposure time (months)[a]	0 to 240
	Maximum temperature (°C)[a]	Time series of Goiânia, GO from 2002 to 2022 (between 23.0 and 37.1) + SARIMA (prediction)
	Minimum temperature (°C)[a]	Time series of Goiânia, GO from 2002 to 2022 (between 13.6 and 23.0) + SARIMA (prediction)
	Relative air humidity (%)[a]	Time series of Goiânia, GO from 2002 to 2022 (between 31.03 and 90.0) + SARIMA (prediction)
	Atmospheric CO_2 concentration (ppm)[a]	Time series of Mauna Loa from 2002 to 2022 (between 372.15 and 418.21) + SARIMA (prediction)
Output signals	Carbonation depths (mm)[a]	Time series from 2002 to 2022 (between 0.0 and 56.91)

[a] For some variables, only the minimum and maximum values are shown as information for a better understanding of the data normalization processes. The detailed levels of each variable are available in Table A.1 (Appendix A).

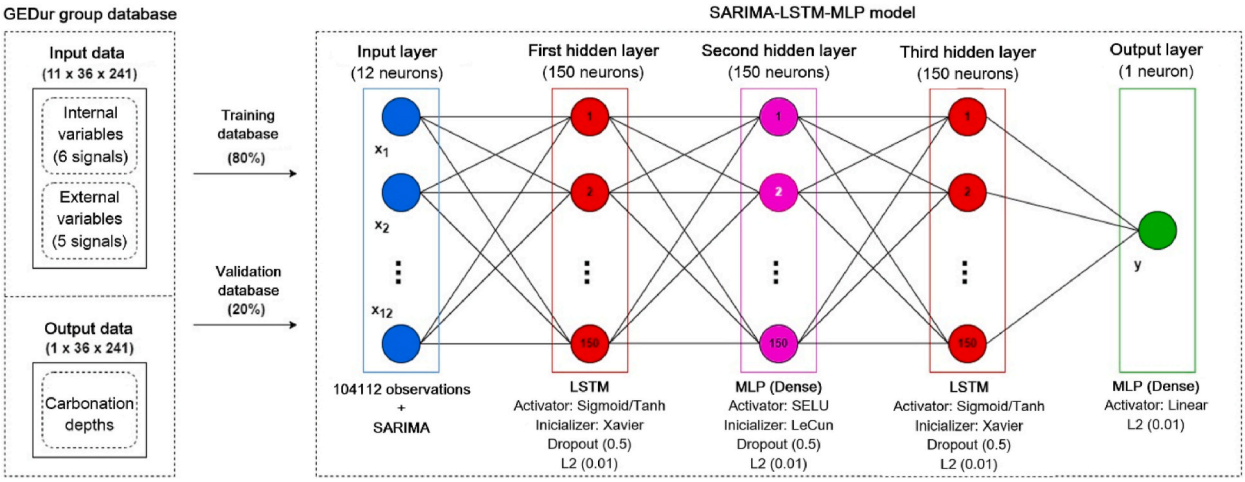

Fig. 6. Architecture of the individual SARIMA-LSTM-MLP predictor models implemented in this study.

model more robust for predictions. The total quantity of data used for training and validation of each individual model was 104,112, with 8676 for each input and output signal. The volume of data used in the training and validation of predictor models reinforces the robustness considered in its construction and implementation process.

After iterative testing with multiple configurations, the setup which yielded the lowest errors and highest stability across the validation datasets was the model contemplating an input layer with twelve neurons (equivalent to the total number of input signals), three hidden layers with 150 neurons each, and an output layer with one neuron (equivalent to the total number of output signals), as illustrated in Fig. 6. The hidden layers present different topologies, where the first and third are LSTM and the intermediate MLP. The output layer is of the MLP type, whose function is to compare the depths labeled and estimated by the SARIMA-LSTM-MLP models.

All the main hyperparameters established for each layer are described in Fig. 6, including activation functions to allow learning of complex characteristics; synaptic weight initializers to adjust the scale of the normal distribution based on the mean number of input and output units; dropouts to enable shutdown of some neurons and avoid overfitting; and L2 regularization to add penalties to the loss function, avoiding underfitting.

The architecture of the SARIMA-LSTM-MLP models can deal with problems involving data sequences with long-term time dependencies. Therefore, a Backpropagation Through Time (BPTT) training algorithm was implemented, which is a variation of BP usually applied to recurrent neural networks. In short, the hyperparameters were selected to ensure the best performance of the models, and their detailed information is presented in Table 4.

A small justification is important regarding the considered dropout of 0.5. The dropout parameter was carefully balanced against

Table 4
Hyperparameters selected after adjustments made during the training and validation phases of the individual SARIMA-LSTM-MLP predictor models.

Training database		80 %
Validation database		20 %
Input and output signals		See Table 3
Data normalization process		Z-score
Artificial neural networks architecture		Hybrid – SARIMA-LSTM-MLP
Training algorithm		BPTT
Activation function	LSTM hidden layers	Sigmoid/Hyperbolic tangent
	MLP hidden layer	SELU
	MLP output layer	Linear
Stop criteria		Early stopping
Training rounds		1
Epochs		3000
Patience		600
Dropout		0.5
Regularization		L2
Batch size		1
Sequence size		12
Optimization algorithm		SGDm
Error metrics		MSE
Python version		3.11.7

the network's ability to learn temporal dependencies. In the LSTM models used in this study, different dropout values were tested, starting from 0.1. The best results - both in terms of prediction accuracy and generalization - were obtained with a dropout rate of 0.5. Additionally, regularization was applied in other parts of the neural network, such as in the intermediate dense (MLP) layer, without significantly impairing the model's ability to capture long-term dependencies.

After training, the SARIMA-LSTM-MLP predictor models were properly validated and underwent performance analyses as described in section 2.2, considering the actual and predicted observations within the validation subset. After prediction, all outputs were transformed back to their original scale using the inverse Z-score transformation: $x = \hat{x}.\sigma + \mu$, where σ and μ are the standard deviation and mean used during normalization.

2.3.2. *Ensemble predictor metamodel*

This section presents the tasks related to step 6 of Fig. 3

The 36 individual SARIMA-LSTM-MLP predictor models were identical by topology/architecture and were highly complex, effectively capturing nonlinear behavior patterns. Therefore, a simplified clustering method defined as average (AVR) was adopted that averages the combined predictions according to new input signals. Thus, individual predictor models began to contribute to the development of a single predictor metamodel identified as AVR-SARIMA-LSTM-MLP. Fig. 7 shows the simplified metamodel construction scheme based on the ensemble topology.

The process of building and implementing the predictor metamodel consisted of combining the individual models, requiring input and output signals only in the testing and generalization phases. The input signals configure the variables adopted in this study (Fig. 2), while the outputs are important for the AVR-SARIMA-LSTM-MLP ensemble predictor metamodel that can perform data normalization and denormalization tasks.

A fundamental aspect of the robustness of the individual predictor models and metamodel proposed in this study was the validation by historical backcasting. This approach consisted of using real data collected during the 20 years of natural exposure of concrete to carbonation during training and validation. The models were able to reconstruct known trajectories of carbonation progression, making it possible to compare the predicted values with the values measured over time. This historical validation was essential to prove the models' ability to accurately capture the phenomenon's past behavior, ensuring consistency with expected patterns - such as the three stages of carbonation identified in the time series analysis [4] - and reinforcing the reliability of future predictions.

The predictions obtained from this metamodel (as well as from the 36 individual SARIMA-LSTM-MLP predictive models) are indeed extrapolative, based on trends derived from long-term exposure data. To ensure reliability, the models were validated on subsets with well-established long-term progression patterns and tested for stability under sudden variations.

2.3.3. *Generalization of ensemble predictor metamodel*

This section presents the tasks related to step 4 of Fig. 3.

The AVR-SARIMA-LSTM-MLP metamodel was generalized by applying new concrete carbonation databases from different studies. This step aimed to evaluate the potential of the metamodel to capture the dynamics of natural carbonation of concretes with different compositions and exposure conditions, in addition to accurately predicting the carbonation fronts. The selection of databases for generalization was based on three assumptions: *i)* completeness of the database, i.e., whether the information was consistent with the input and output signals of the AVR-SARIMA-LSTM-MLP predictor metamodel; *ii)* exposure time, with preference given to collections with longer exposure times of concretes to natural carbonation; and *iii*) geographical location, to explore concretes subjected to exposure conditions of different Brazilian climate zones.

Thus, three distinct databases were selected:

- **Meira, Padaratz, and Borba Júnior** [85] studied the natural carbonation of concrete pillars after four years of exposure distributed in different locations, 10, 100, 200, and 500 m away from the sea, in the city of João Pessoa, PB, in the Brazilian climatic

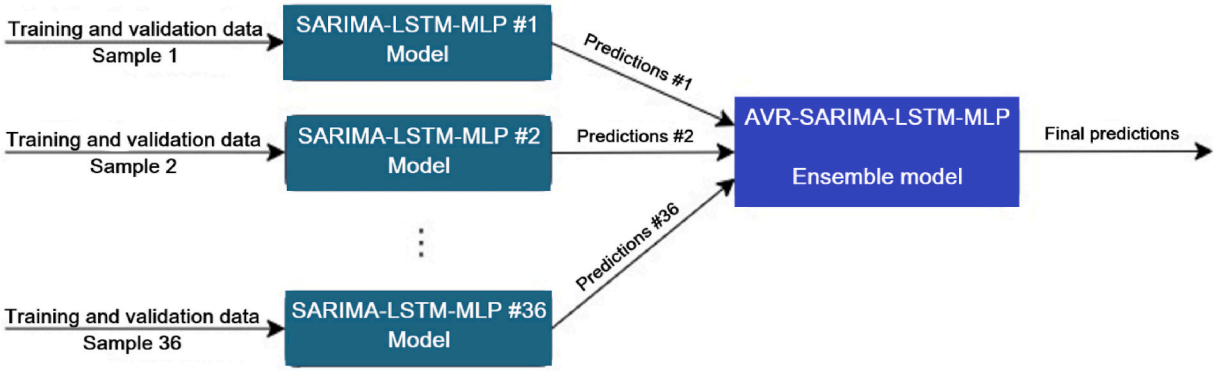

Fig. 7. Simplified implementation scheme of the AVR-SARIMA-LSTM-MLP ensemble predictor metamodel.

zone Tropical Northeastern East. The specimens were subjected to wet curing for 7 days, and the carbonation depths were measured at 6, 10, 14, 18, and 46 months.

- **Pauletti** [86] evaluated accelerated and natural carbonation of prismatic mortar specimens after almost five years of exposure. The specimens exposed to natural carbonation were distributed in three different locations: two outdoor environments not protected from the weather (São Leopoldo, on the Unisinos campus, and Porto Alegre, next to Noire) and one in an air-conditioned room at 20 $\pm$ 1 °C and 70 $\pm$ 5 % RH with a CO_2 concentration of 880 ppm. Both cities are located in the Brazilian Temperate climate zone. The specimens were subjected to wet curing for 28 days, and the carbonation depths were measured at 6, 14, 20, 30, 48, and 58 months.
- **Tasca** [87] **and Silveira** [88] include a master's thesis and a doctoral thesis, respectively, supervised by Prof. Dr. Geraldo C. Isaia. Both address studies of natural carbonation of the same concretes (with pozzolanic addition) with 14 and 20 years of exposure. The concretes were produced in 1997 by Vaghetti [89]. They were kept conserved and sheltered in a covered and closed environment in Santa Maria, RS, in the Brazilian Temperate climate zone. The carbonation depths were measured at 12, 24, 48, 168, and 240 months.

Table A.2 of Appendix A the list the identifications adopted for the concretes of the generalization databases and the complete information about the input signals provided by the respective authors. Samples 1 to 36 comprise the concretes of the GEDur group database; therefore, the identifications of the sample for generalization power studies of the ensemble predictor metamodel start from number 37. Water absorption values were estimated by linear prediction based on f_{ck} values, respecting the type of mineral addition and w/b ratio.

To perform analyses, the prediction results generated by the AVR-SARIMA-LSTM-MLP metamodel were compared with the actual carbonate depths available in the databases. Analyses were performed following the criteria presented in section 2.2.

3. Results and discussion

For better organization and presentation of results and discussions, this section has been divided into three major parts.

- **Analysis and predictions of climatic and environmental time series**: The results of investigations and predictions of the time series of maximum temperature, minimum temperature, relative humidity, and atmospheric concentration of CO_2 are presented using time series analysis techniques.
- **Prediction with the individual SARIMA-LSTM-MLP models**: The results and analysis of the predictions of the natural carbonation depths obtained with the individual predictor models.
- **Prediction with the ensemble metamodel AVR-SARIMA-LSTM-MLP**: The results and analysis of the predictions of carbonation depths and generalization power recorded by the ensemble predictor metamodel are presented.

To ensure better organization and ease in presenting the results, the 36 concretes of the GEDur group were sampled. The samples were selected, so that all variables associated with the composition and curing condition of the concretes were considered. The samples selected were R4W (1), M5W (11), FA7W (15), RHA4W (16), R4D (19), BFS7D (24), and SF5D (26) (see Table 1).

3.1. Analyses and previsions of climate and environmental time series

3.1.1. Climate parameters of Goiânia, GO, and environmental parameters of Mauna Loa

Considering the monitoring of the climatic and environmental variables in an aging environment of the concrete beam prototypes throughout 2023, the data collected in the environment were statistically compared to the data recorded by the meteorological station of Goiânia, GO, and the Mauna Loa Observatory. Correlation coefficients of 0.88, 0.99, and 0.50 were recorded for temperature, air humidity, and CO_2 concentration, respectively. As expected, temperature and humidity measured in the aging environment show excellent correlations with weather station climate data. The correlation between the CO_2 concentrations collected in the aging

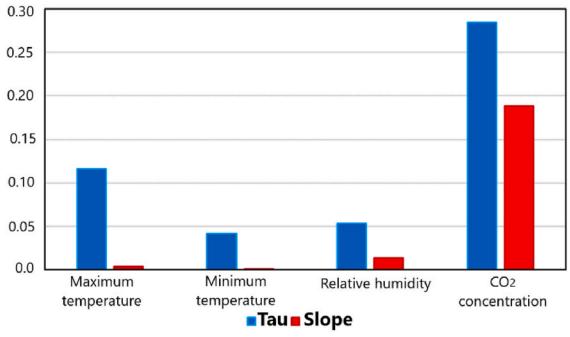

Fig. 8. Tau and slope results of climate and environmental variables between April 2002 and March 2022 based on data from weather station in the Goiânia, GO, Brazil (code 83423 – INMET [69]) and released by NOAA [70].

environment and those recorded by NOAA [70] was expected to be lower, as these values were recorded in completely different environments. We decided to maintain the values recorded by the observatory, as they are within the limits established in the relevant literature [22,23]. The graphs with the monthly values monitored throughout 2023 and the values from the institutions are available in Appendix B.

To predict the carbonation fronts, the maximum and minimum temperatures, relative humidity, and CO_2 concentration data were subjected to TSA and subsequently inserted as input signals in the SARIMA-LSTM-MLP predictor models. The TSA elucidated that all climatic and environmental parameters present gradual increase or decrease trends over the years. Fig. 8 shows the results of Tau (measurement of the correlation of data over time) and slope (slope of the trend line), considering the data between April 2002 and March 2022.

CO_2 concentration showed the strongest trend and the highest slope of all the parameters. Among the climatic parameters, the maximum temperature produced the strongest trend, while air humidity exhibited the greatest slope. Thus, in the region of Goiânia, GO, the maximum temperature tends to increase more than the minimum, while air humidity tends to reduce with greater intensity over the years. These results demonstrate that adopting fixed means to feed ANN-predictor models can bias the results because all climatic and environmental parameters present significant variations in the long term. Thus, the predictions of the time series of these variables were made in a period equal to that sought to predict the carbonation phenomenon of the concretes.

Predictions cover until to the year 2100 by applying SARIMA (p, d, q) (P, D, Q) S. Fig. 9 illustrates the results of the predictions of maximum and minimum temperatures, air humidity, and CO_2 concentration. The orders of autocorrelation, differentiation, and moving average (p, d, q); seasonal autocorrelation, seasonal differentiation, seasonal moving average (P, D, Q); and seasonal period (S) defined using the AIC criterion, whose lowest values indicated the best model to represent the prediction. The results of the orders that best fit each climatic and environmental parameter are described in Table 5.

The trend and seasonality components of the maximum and minimum temperatures and relative air humidity were adequately captured. The temperatures showed increasing trends – more marked at the maximum temperature – and humidity showed a

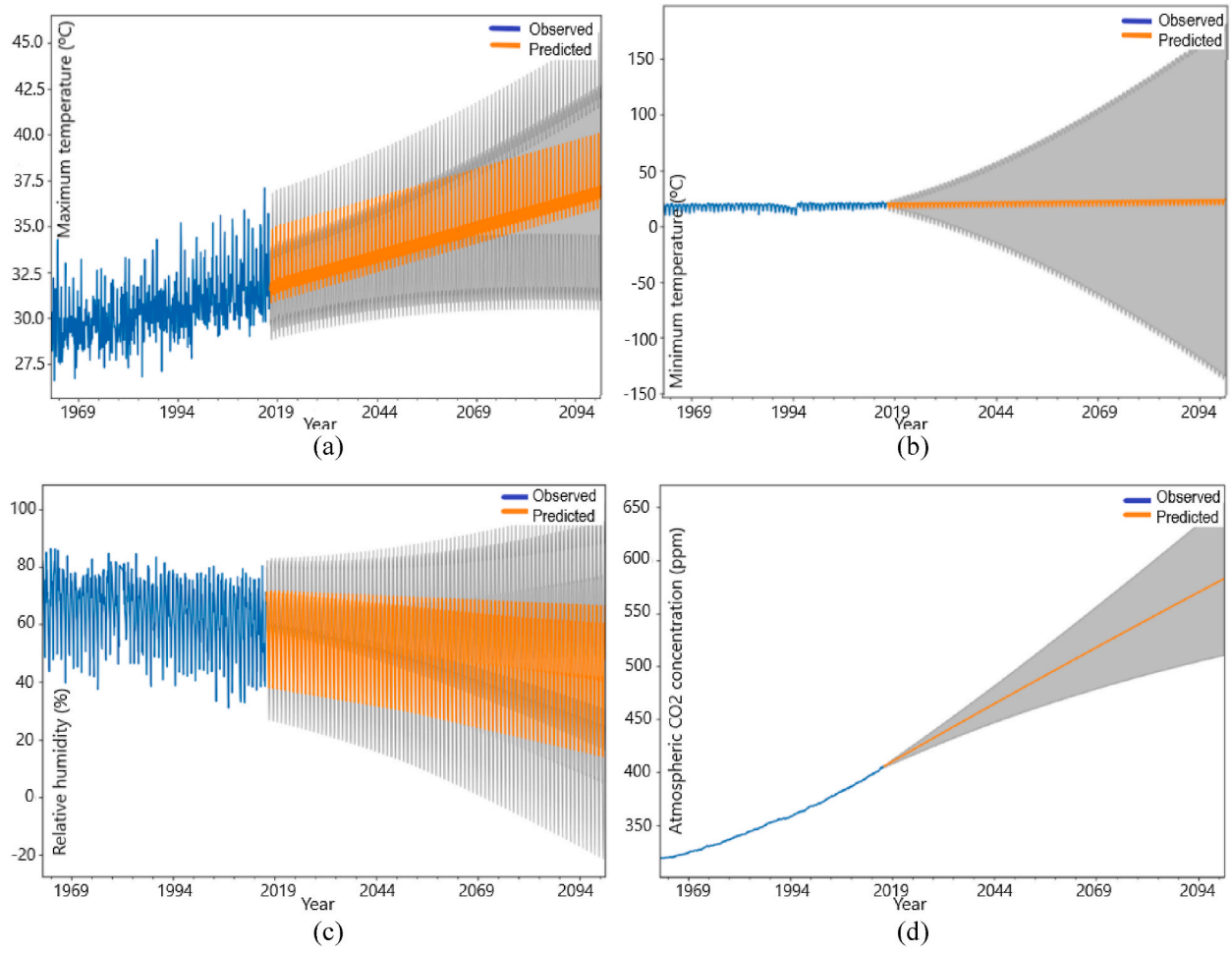

Fig. 9. Results of the predictions of maximum (a) and minimum (b) temperatures, relative air humidity (c), and atmospheric CO_2 concentration (d) for the aging environment of concrete beams prototypes using SARIMA (p, d, q) (P, D, Q) S.

Table 5
SARIMA models (p, d, q) (P, D, Q) S and the respective orders with lower AIC values used to predict the climatic and environmental parameters related to the aging environment of the prototype concrete beams of the GEDur group.

Climatic and environmental parameters	SARIMA (p, d, q) (P, D, Q, S) models
Maximum temperature	SARIMA (1, 1, 2) (2, 1, 2, 12)
Minimum temperature	SARIMA (0, 1, 1) (1, 1, 1, 12)
Relative air humidity	SARIMA (1, 0, 2) (0, 2, 2, 12)
Atmospheric CO_2 concentration	SARIMA (1, 0, 1) (0, 1, 1, 12)

Table 6
Results of the performance analysis of climate/environmental data predictions.

Climatic and environmental parameters	RMSE (Root Mean Square Error)	d (Agreement index)	R (Correlation coefficient)	c (Performance index)
Maximum temperature	0.97	0.88	0.85	0.75
Minimum temperature	0.79	0.96	0.94	0.90
Relative air humidity	4.48	0.97	0.94	0.90
Atmospheric CO_2 concentration	0.60	0.99	0.99	0.99

decreasing trend. The same could be observed in the CO_2 concentration, as the slope of the trendline of this parameter is considerably higher.

To measure the quality of the SARIMA prediction models, performance analyses were performed, and the results are presented in Table 6. In all performance criteria, the predictive models based on TSAs recorded satisfactory results, with a very good level for the maximum temperature and optimal levels for the other variables, as established in Table 2. Based on the predictions, if nothing is done to contain the advance of global warming, by 2100, the temperature will increase by approximately 4.8 °C and CO_2 concentration by about 166 ppm. These values fit neatly into category C8 (SSP5-8) of the AR6 report from IPCC [79]. Finally, all predicted climatic and environmental time series were used as input signals of the SARIMA-LSTM-MLP predictor models of the concrete carbonation fronts.

3.1.2. Climate parameters of Brazilian capitals

The same analyzes applied to the climatic parameters of Goiânia, GO, were carried out for several Brazilian capitals. This permitted the evaluation of the generalization power of the AVR-SARIMA-LSTM-MLP ensemble predictor model to consider the climatic data most consistent with the respective concrete storage locations.

Table 7
Results of the Brazilian capitals selected for predicting cities with related climates, and the SARIMA predictive models (p, d, q) (P, D, Q) S with lower AIC values.

Climate zone	City/State	Cities with similar climates	Climatic parameters	SARIMA (p, d, q)(P, D, Q)S models
Equatorial	Manaus/AM	Belém/PA	Maximum temperature	SARIMA (1, 0, 1) (0, 1, 1, 12)
		Macapá/AP	Minimum temperature	SARIMA (1, 1, 1) (0, 1, 1, 12)
		Rio Branco/AC	Relative air humidity	SARIMA (1, 0, 1) (0, 1, 1, 12)
Tropical Equatorial	Boa Vista/RR	–	Maximum temperature	SARIMA (1, 1, 1) (0, 1, 1, 12)
			Minimum temperature	SARIMA (1, 1, 1) (0, 1, 1, 12)
			Relative air humidity	SARIMA (1, 1, 1) (0, 1, 1, 12)
Tropical Equatorial	Fortaleza/CE	São Luís/MA	Maximum temperature	SARIMA (1, 1, 1) (0, 1, 1, 12)
		Teresina/PI	Minimum temperature	SARIMA (1, 0, 1) (1, 1, 1, 12)
			Relative air humidity	SARIMA (1, 1, 1) (0, 1, 1, 12)
Tropical Oriental Northeast	Recife/PE	Aracajú/SE	Maximum temperature	SARIMA (1, 1, 1) (0, 1, 1, 12)
		João Pessoa/PB	Minimum temperature	SARIMA (1, 0, 1) (0, 1, 1, 12)
		Maceió/AL	Relative air humidity	SARIMA (1, 1, 1) (0, 1, 1, 12)
		Natal/RN		
		Salvador/BA		
Tropical Brazil Central	Goiânia/GO	Belo Horizonte/MG	Maximum temperature	SARIMA (1, 1, 2) (2, 1, 2, 12)
		Brasília/DF	Minimum temperature	SARIMA (0, 1, 1) (1, 1, 1, 12)
		Cuiabá/MT	Relative air humidity	SARIMA (1, 0, 2) (0, 2, 2, 12)
		Palmas/TO		
Tropical Brazil Central	São Paulo/SP	–	Maximum temperature	SARIMA (1, 1, 1) (0, 1, 1, 12)
			Minimum temperature	SARIMA (1, 1, 1) (0, 1, 1, 12)
			Relative air humidity	SARIMA (1, 1, 1) (0, 1, 1, 12)
Tropical Brazil Central	Vitória/ES	–	Maximum temperature	SARIMA (1, 0, 1) (0, 1, 1, 12)
			Minimum temperature	SARIMA (1, 0, 1) (0, 1, 1, 12)
			Relative air humidity	SARIMA (1, 1, 1) (0, 1, 1, 12)
Temperate	Florianópolis	Curitiba/PR	Maximum temperature	SARIMA (1, 0, 1) (0, 1, 1, 12)
	/SC	Porto Alegre/RS	Minimum temperature	SARIMA (1, 0, 1) (0, 1, 1, 12)
			Relative air humidity	SARIMA (1, 1, 1) (1, 1, 1, 12)

The correlations between the climates of all capitals were evaluated, separating the capitals by Brazilian climate zones and using the histories of air humidity and maximum and minimum temperatures published by INMET [69]. One capital was considered to have a climate correlated to another only if two of the three climate variables had a correlation coefficient (R) equal to or greater than 0.60. This value was adopted because it indicates a moderate to strong correlation and, consequently, a substantial relationship between the climates of different cities. Based on this premise, eight capitals were selected that represent all the others in their respective climate zones. Subsequently, climate predictions were carried out until the year 2100 applying the SARIMA predictor model, as well as data from Goiânia, GO. The results of the correlations between the capitals and the orders that best adjusted the climate predictor models of each city are described in Table 7.

Thus, these climate data and their respective predictions, associated with the carbonation databases of the various studies, were used to predict the carbonation fronts and evaluate the power of generalization of the knowledge of the AVR-SARIMA-LSTM-MLP ensemble metamodel.

3.2. *Predictions with the individual SARIMA-LSTM-MLP models*

During the training and validation phases of the 36 individual SARIMA-LSTM-MLP predictor models, graphs were generated that depict the results of the predictions and the evolution of errors throughout the process. Fig. 10 are two graphs resulting from training and validation for sample 1 (R4W), including *i)* values used in training (in blue), validation (in green and orange), and predicted values (in red); *ii)* results of the evolution of prediction errors during training (in blue) and validation (in red). Appendix C presents the results of the predictions and evolutions of the errors of the selected concretes for presentation and discussion of the results in Table 1.

Carbonated depth prediction works with ANN-based models to validate the models only based on the data from the validation subsets, imagining that the machine fully captured the evolutionary profile of the phenomenon. However, the prediction results of ANN-based models should be associated with time series analyses to validate whether the predictions are consistent with the expected behavior of the phenomenon. This is especially true when using databases with less than 10 or 12 years of exposure to natural carbonation, as they do not cover all stages of the phenomenon identified in the work of Campos Neto [4] and presented in Fig. 1. Thus, knowledge about the profile of the carbonation curve in the long term helped establish the expected evolution of the phenomenon, serving as a complementary validation of the results presented by the predictive models based on ANNs. In addition, understanding the evolutionary pattern of carbonation allows the adjustment of hyperparameters and general configurations of artificial neural networks to ensure greater accuracy and precision.

In this study, the predictions (with the individual SARIMA-LSTM-MLP models) were carried out until the month number 1027, i.e., almost 86 years after the production of the concretes (April 2002) by Castro [67]. Fig. 10 indicates that the prediction results are compatible with those expected from the time series analysis because, after about 10–12 years of exposure, the phenomenon tends to stabilize the depths of carbonation, entering stage III (Fig. 1). Furthermore, as in the real domain, the carbonation profile predicted by the SARIMA-LSTM-MLP model tends to stabilize but does not reach total suspension, maintaining a slow advance in the long term. Regarding the errors, the results were satisfactory because, as expected, the highest values were recorded in the training phase and the lowest in the validation phase. Thus, the individual SARIMA-LSTM-MLP predictor models adequately captured the evolutionary pattern of carbonation during training, being efficiently applied in validation. The error metric is the MSE, with unit in mm^2, and after 500 training times, all errors were less than 0.5 mm^2, equivalent to 0.71 mm. Only sample 24 (BFS7D) presented higher errors,

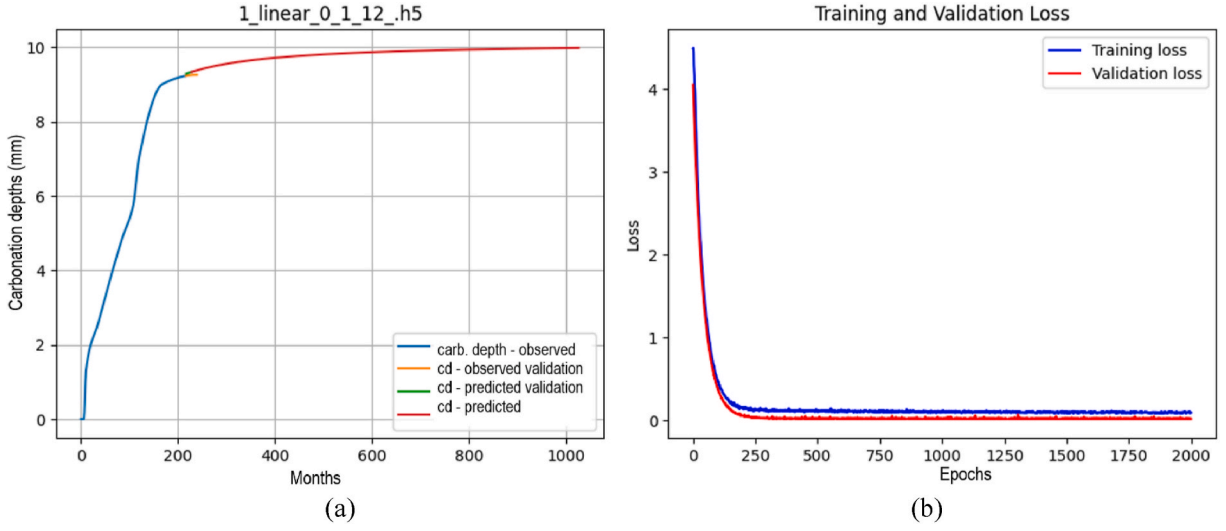

Fig. 10. Results generated during the training and validation process of the SARIMA-LSTM-MLP individual predictor model of sample 1 (R4W). The graphs show the actual (blue and orange) and predicted (green and red) values of the carbonation depths (a) and the evolutions of the training errors (blue) and validation (red) of the model (b).

Table 8
Results of the correlation coefficients (R), determination (R^2), and RMSE of the validation subsets of the actual and predicted carbonate depths by the individual SARIMA-LSTM-MLP models for samples 1 (R4W), 11 (M5W), 15(FA7W), 16 (RHA4W), 19 (R4D), 24 (BFS7D), and 26 (SF5D).

Sample 1		**Sample 11**		**Sample 15**		**Sample 16**	
R	0.9969	R	0.9985	R	0.9998	R	0.9999
R^2	0.9939	R^2	0.9971	R^2	0.9997	R^2	0.9998
RMSE	0.069	RMSE	0.027	RMSE	1.631	RMSE	0.084
Sample 19		**Sample 24**		**Sample 26**			
R	0.9962	R	0.9996	R	0.9999		
R^2	0.9924	R^2	0.9993	R^2	0.9998		
RMSE	0.018	RMSE	7.906	RMSE	0.273		

reaching 0.8 mm^2 or 0.89 mm, which is still within the acceptable range adopted in the literature for concrete carbonation metrics of between 4.0 mm and 5.0 mm [90,91].

Results from the analysis based on the predicted values within the validation subset of the SARIMA-LSTM-MLP models are presented in Table 8. Observe that all R were greater than 0.99, and the minimum and maximum coefficients of determination (R^2) were equal to 0.9924 and 0.9999, respectively. Considering the results of the 36 individual predictor models implemented for the concretes of the GEDur group, the mean, standard deviation, and coefficient of variation of the R were equal to 0.999, 0.001, and 0.127, respectively. This verifies that the predictions strongly correlate with the actual carbonate depths, regardless of the w/b ratio, type of mineral addition, and curing condition of the concretes. In addition, the RMSE values were within the acceptable theoretical limits for carbonation, except again for sample 24 (E70). RMSE is sensitive to extreme values, where a single observation can increase it, even if the model is accurate. This may explain what happened with sample 24 (E70) because even after 14 years, its depth significantly increased, which is not characteristic of the evolutionary pattern of concrete carbonation.

These data indicate that the individual SARIMA-LSTM-MLP predictor models implemented for the GEDur group concretes could be used as a digital foundation for the ensemble predictor model. Therefore, all 36 files with. h5 extension were combined in a metamodel to increase the predictive capacity.

3.3. Predictions with the ensemble metamodel AVR-SARIMA-LSTM-MLP

The ensemble predictor metamodel AVR-SARIMA-LSTM-MLP was employed to predict the carbonation fronts of the 36 concretes of the GEDur group, the 12 concretes of Meira, Padaratz and Borba Júnior [85], the 18 concretes of Pauletti [86], and the 12 concretes of Tasca [87] and Silveira [88], totaling 78 different samples. Using it, graphs and tabulated numerical data were generated with an estimated 806 months, i.e., more than 67 years after the production of the concretes. First, linear regression analyzes were performed between the actual and predicted observations considering all available carbonate depths, i.e., from the production of the concretes (time zero) to the limit months available in the respective databases.

Taking all R values, the tree map in Fig. 11 shows that more than half of the concretes – about 56.4 % - registered R equal to or greater than 0.95; around 24.36 % presented R between 0.90 and 0.949; 11.54 % between 0.85 and 0.899; 3.85 % between 0.80 and 0.849; and 3.85 % below 0.80. In other words, only 3 of the 78 concretes had R lower than 0.80. The mean, standard deviation, and coefficient of variation of the R values of all concretes are equal to 0.93, 0.07, and 6.92, respectively. Hence, the predictor metamodel AVR-SARIMA-LSTM-MLP presented results with low variability and very strong correlation with the real observations, suggesting its fitness.

Although the correlation coefficient can indicate the strength and direction of the relationship between two data sets, it does not provide information about the accuracy of ensemble metamodel predictions. Therefore, complementary performance analyses were carried out – as established in section 2.2 – for concretes with the high, intermediate, and low R values. From the GEDur group, the

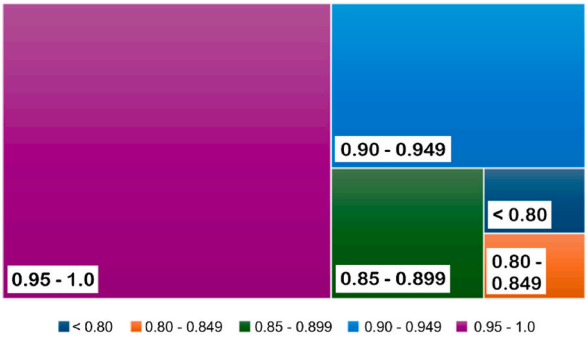

Fig. 11. Treemap with the results of the correlation coefficients (R) between the actual and predicted carbonate depths by the AVR-SARIMA-LSTM-MLP ensemble metamodel for the 78 concretes (36 from the GEDur group and 42 from other researchers).

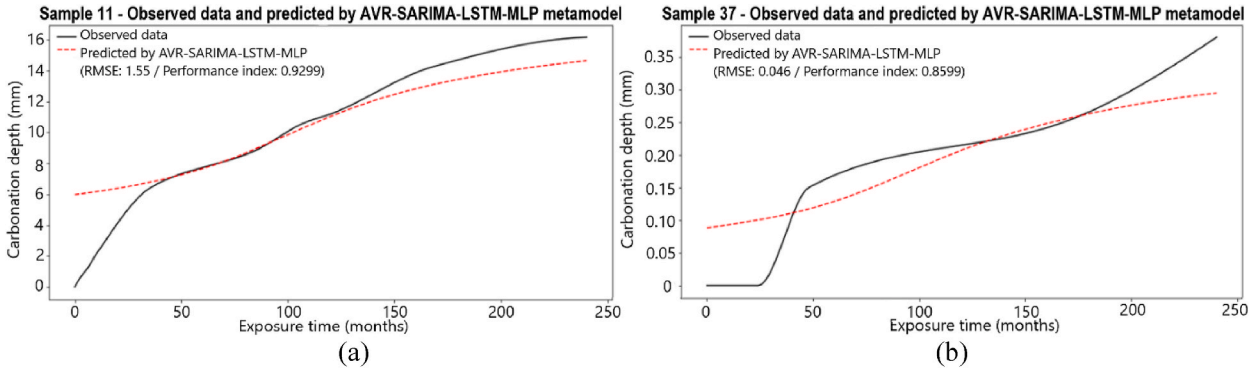

Fig. 12. Results of the observed curves (solid lines in black) and predicted (dashed lines in red) by the AVR-SARIMA-LSTM-MLP ensemble model based on data from 20 years of exposure to natural carbonation of samples 11 (M5H) from the GEDur group (a), and 37 from Tasca [87] and Silveira [88] (b).

same seven samples already considered in the previous steps were used (Table 1); from Tasca [87] and Silveira [88], samples 37, 40, 44, and 46 were selected; from Meira, Padaratz, and Borba Júnior [85], samples 50, 52, 54, and 59 were selected; and from Pauletti [86], samples 61, 69, 70 and 77 were selected, all as identified in Table A.2 of Appendix A.

Fig. 12 presents some of the carbonation curves based on real observations (continuous lines in black) and predicted by the AVR-SARIMA-LSTM-MLP ensemble metamodel (dashed lines in red) for the concretes of the GEDur and Tasca [87] and Silveira [88] groups. This visualization shows that the metamodel managed to capture the evolutionary pattern of concrete carbonation, with lower initial depths that rise and tend to stabilize over the months. These graphs are a first glimpse that the ensemble predictor metamodel has great potential to generate knowledge, as it can predict the phenomenon even for concretes with different characteristics and properties, which were subject to different exposure conditions.

For the first ages, the AVR-SARIMA-LSTM-MLP metamodel predicted high values, which indicated that it identified the accelerated initial advance of the carbonation fronts. Thus, we sought to determine the time elapsed between the beginning of the phenomenon and the intersection point of the two curves – which represents the lowest error value. The average time found is 4.05 years, that is, exactly the same period established for stage I of carbonation (Fig. 1). The focus of this work was to analyze carbonation in terms of concrete durability by creating an ensemble predictor metamodel with its greatest errors only in the first four years and subsequently exhibiting the minimum possible; therefore, the model is effective for what is proposed. This pattern was verified in all 78 concretes studied.

These hypotheses can be confirmed by verifying the results of the performance analyses (Table 9). The values of RMSE, d (agreement index), c (performance index), and performance class are arranged according to Table 2.

The performance classes recorded were between good and great, with performance indices – which associate precision and accuracy metrics – equal to or greater than 0.67. The RMSE values recorded by the Tasca [87] and Silveira [88] samples were lower than those of the GEDur group samples. Therefore, the AVR-SARIMA-LSTM-MLP metamodel presented high generalization power for the accuracy of the predictions of the carbonation fronts of concretes different from those used in the training and validation. All RMSEs were less than 4.69 mm; thus, within acceptable limits for carbonation. Therefore, the ensemble predictor metamodel can capture different evolutionary patterns of the phenomenon and precisely and accurately predict the carbonated depths of concretes with

Table 9
Results of the performance analysis of the predictor metamodel ensemble AVR-SARIMA-LSTM-MLP based on data from 20 years of exposure to natural carbonation of samples from the GEDur group and Tasca [80] and Silveira [88] group.

Samples	RMSE (Root Mean Square Error)	d (Agreement index)	c (Performance index)	Performance class
Concretes of GEDur group				
1	2.95	0.68	0.67	Good
11	1.55	0.95	0.93	Excellent
15	3.90	0.95	0.93	Excellent
16	0.89	0.94	0.90	Excellent
19	0.94	0.89	0.76	Very good
24	4.69	0.93	0.87	Excellent
26	2.45	0.94	0.90	Excellent
Concretes of Tasca [87] and Silveira [88]				
37	0.05	0.93	0.86	Excellent
40	1.03	0.92	0.85	Very good
44	0.16	0.84	0.82	Very good
46	2.12	0.84	0.82	Very good

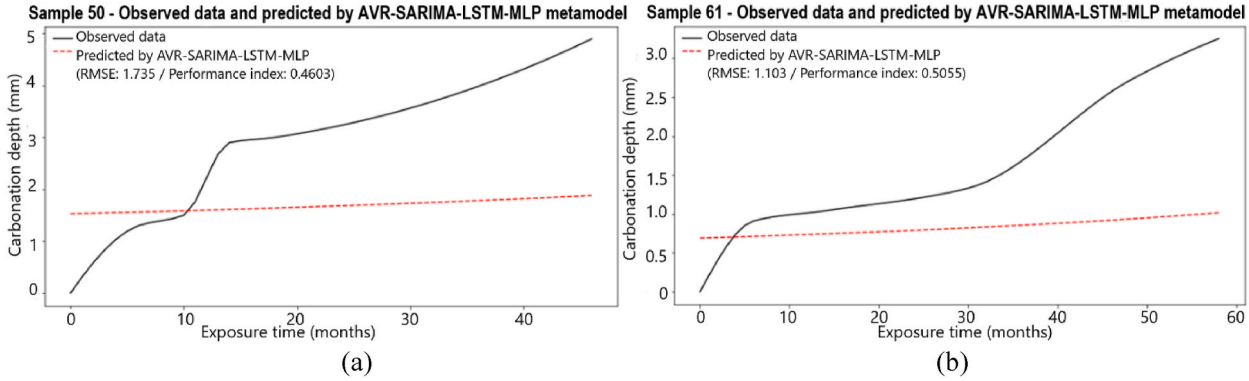

Fig. 13. Results of the observed (solid lines in black) and predicted (dashed lines in red) curves by the AVR-SARIMA-LSTM-MLP model based on data from almost 4 years of exposure to natural carbonation of sample 50 of Meira, Padaratz, and Borba Júnior [85] (a) and nearly 5 years of exposure of sample 61 of Pauletti [86] (b).

Table 10
Results of the performance analyses of the AVR-SARIMA-LSTM-MLP metamodel based on data from almost 4 and 5 years of exposure to natural carbonation of the samples from Meira, Padaratz, and Borba Júnior [85] and Pauletti [86], respectively.

Samples	RMSE (Root Mean Square Error)	d (Agreement index)	c (Performance index)	Performance class
Concretes of Meira, Padaratz and Borba Júnior [85]				
50	1.74	0.49	0.46	Poor
52	1.73	0.51	0.49	Poor
54	3.60	0.50	0.49	Poor
59	2.68	0.49	0.46	Poor
Concretes of Pauletti [86]				
61	1.10	0.52	0.51	Sufferable
69	0.77	0.41	0.24	Bad
70	4.41	0.51	0.49	Poor
77	2.47	0.51	0.47	Poor

different characteristics, properties, curing conditions, and exposure.

It is important to note that the concrete produced with blast furnace slag (sample 24) showed the highest RMSE value. This behavior, which differs from the standard curve, may reflect the increase in capillary porosity resulting from the decomposition of the matrix's C-S-H exposed for long periods to CO_2, as studied by Ngala and Page [92]. In the physical dimension, Martins [93] identified an increase in air permeability in concrete with the addition of blast furnace slag, which contributed to the irregular advance of carbonation fronts.

For the databases of Meira, Padaratz, and Borba Júnior [85] and Pauletti [86], Fig. 13 shows the actual and predicted curves, and Table 10 provides the results of the performance analyses. Notably, regardless of the database, the predicted curves did not exhibit the same slope pattern as the actual curves. All observed curves presented values higher than those predicted, with a greater slope, indicating a more accelerated process than estimated. Furthermore, the indices and performance classes were lower, being between poor and very poor. Therefore, at first, visual analysis and performance results indicate that the metamodel did not present satisfactory results, with its power of generalization compromised.

However, it is essential to emphasize that the focus of this work was to contemplate the durability of concrete, i.e., to focus on time as one of the main research variables. Thus, using a database with exposure time limited to stage I of carbonation can influence the ensemble metamodel to adopt values lower than the real ones due to the absence of superior data equivalent to advanced ages. Consequently, the performance classes were impaired by the lack of data referring to stages II and III, which, if available, would have allowed a stronger correlation to be established due to the long-term capture of the evolutionary pattern of concrete carbonation. This emphasizes the importance of the robustness of the database to be used as an input signal for predictive models based on artificial neural networks.

From another perspective, the RMSE values were reduced to between 0.77 and 4.41 mm. Even without adequately capturing the profile of the curve in stage I, the ensemble predictor metamodel AVR-SARIMA-LSTM-MLP presents errors within the limits established by the literature, i.e., between 0.5 and 5.0 mm, making it considered accurate.

To reaffirm the metamodel prediction potential, Fig. 14 illustrates the carbonation curves of some samples from the GEDur; Tasca [87] and Silveira [88]; Meira, Padaratz, and Borba Júnior [85]; and Pauletti [86] groups. These curves include the data of the measured depth periods (blue line highlighted in gray) and the predictions (orange line) of the ensemble metamodel for 806 months (approximately 67 years). Appendix D presents the observed and predicted carbonation curves for the other concretes.

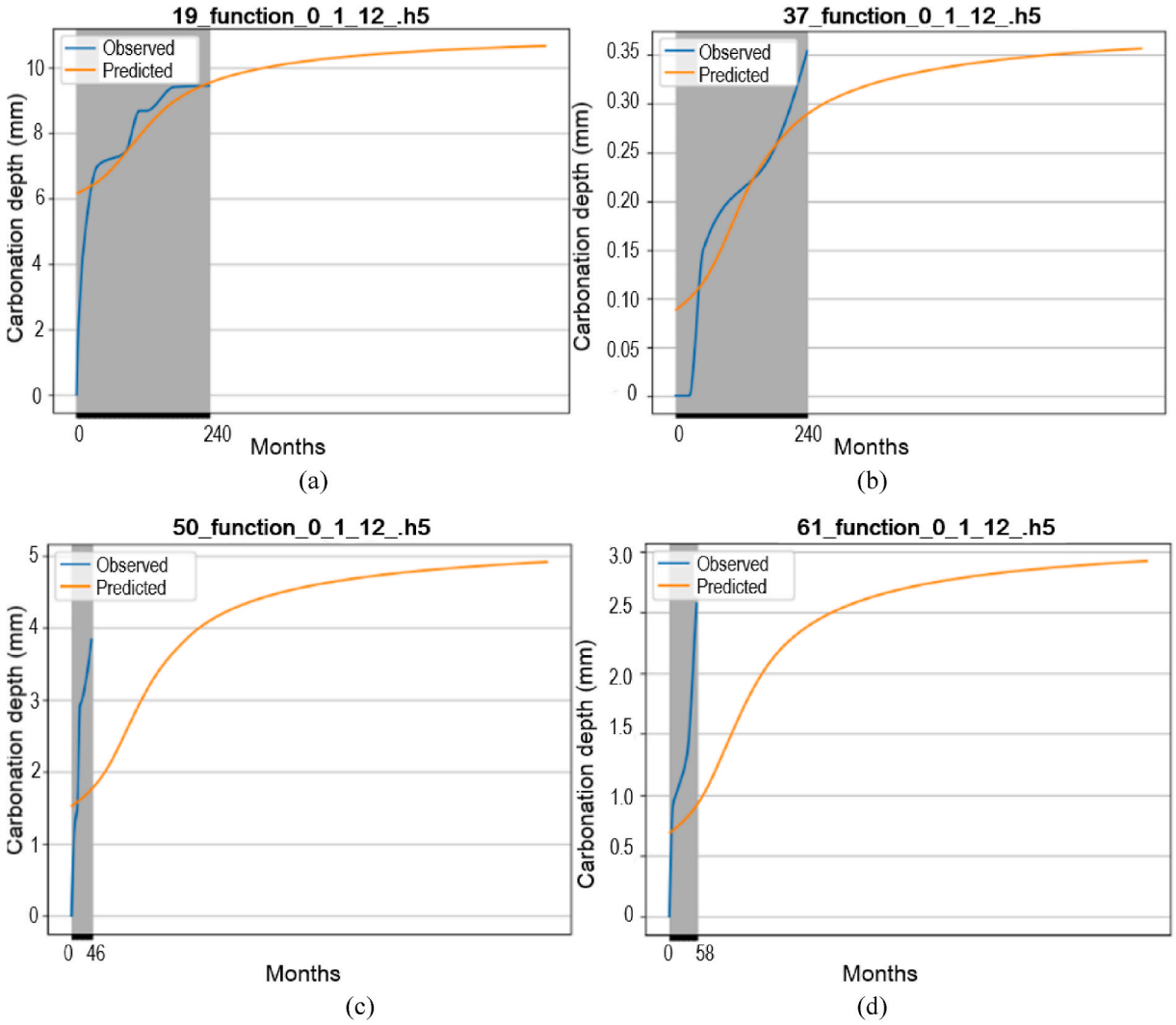

Fig. 14. Results of the curves of observed carbonation depths (lines in blue with gray highlight) and predicted (orange lines) by the ensemble metamodel AVR-SARIMA-LSTM-MLP up to 806 months (approximately 67 years) of samples 19 (R40) from the group GEDur (a), 37 from Tasca [87] and Silveira [88] (b), 50 from Meira, Padaratz and Borba Júnior [85] (c), and 61 from Pauletti [86] (d). The title of each graph notes the sample number, the term function, the round number, the batch and the sequence sizes adopted as part of the artificial neural networks hyperparameters.

As observed in Fig. 14c and d, the deviations between predicted and actual values are more pronounced during the initial carbonation periods. This discrepancy can be attributed to the high variability of Stage I carbonation, as identified by Campos Neto [4], where data dispersion is greater due to the high initial reaction rate. The model tends to exhibit lower accuracy in this interval, reinforcing the importance of training the networks with data that encompasses all stages of the carbonation phenomenon. Even with unsatisfactory performance classes, the carbonation curves predicted for the samples of Meira, Padaratz, and Borba Júnior [85] and Pauletti [86], when analyzed under a longer exposure time, reach the values equal to or higher than those measured by the researchers. Therefore, after about 10 or 12 years of exposure, the data of these researchers should again be submitted to the AVR-SARIMA-LSTM-MLP ensemble predictor metamodel. This indication is necessary because only after this period would the data be sufficient to establish the evolutionary profiles of the carbonation curves in all their stages (Fig. 1).

Nevertheless, for the 78 concretes studied, the predicted carbonation curves were correlated and similar to the real curves. Additionally, the predictions that extrapolated the exposure time of the concretes presented the expected behavior for the different stages of the phenomenon. In other words, the stages – especially stages II and III – of carbonation can be observed with more prominent inclinations in the intermediate ages and a subsequent tendency to stabilize the phenomenon.

In summary, the results achieved with the AVR-SARIMA-LSTM-MLP ensemble metamodel confirm the success of carbonation depth predictions for different types of concretes subjected to different curing conditions and exposed to different climatic and environmental conditions. Its efficiency is based on the remarkable ability to generalize knowledge, becoming a powerful tool to predict carbonation fronts and opening new possibilities for optimizing strategies to maintain and preserve concrete structures.

Associated with time series analyses, integrating data and input variables and understanding the complex relationship between them, the ensemble predictor metamodel AVR-SARIMA-LSTM-MLP overcomes technical challenges and underscores the ongoing importance of interdisciplinary research. This is a significant milestone in advancing durability studies and highlights the relevance of developing intelligent solutions for future civil engineering problems.

While this study focused on natural carbonation, the SARIMA-LSTM-MLP model architecture is also adaptable to simulate accelerated carbonation scenarios if the input data reflects laboratory conditions and parameters associated with accelerated exposure. This adaptation would require reparameterization and retraining of the model using specific datasets; however, the underlying algorithmic structure proposed in this work can be maintained. In addition, the environmental conditions represented in the data refer mainly to the tropical climate of Brazil, whose territorial dimensions are continental but may still limit direct applicability to other regions without prior recalibration and validation of the metamodel. However, only the climatic and environmental time-dependent data need to be recalibrated according to local exposure conditions, while non-temporal variables, such as concrete composition, do not require adjustment.

Even though the AVR-SARIMA-LSTM-MLP metamodel adopted in this study demonstrates excellent predictive performance, it is important to acknowledge the "black-box" nature of deep learning algorithms, which hinders the direct interpretation of the relationships among variables. The formulation of explicit mathematical expressions can be particularly valuable in regulatory contexts and for enhancing physical understanding of the carbonation phenomenon. However, the adoption of symbolic models depends heavily on the quality, temporal extent, and dimensionality of the available data, as well as on the nonlinear complexity of the phenomena involved. Thus, despite not providing symbolic expressions, the proposed metamodel offers significant advantages due to its robustness in handling the high variability of environmental conditions and concrete properties.

4. Conclusions

This study presented a predictor metamodel developed based on a combination of 36 neural networks with a hybrid architecture composed of SARIMA, LSTM and MLP, with the aim of predicting the evolution of carbonation depth in concrete subjected to natural exposure over a 20-year period. The metamodel showed satisfactory performance, with correlation coefficients greater than 0.93 and RMSE values between 0.05 mm and 4.69 mm, demonstrating its ability to capture the relationships among the input variables. The predictions made for extended periods, up to 86 years after the specimens were cast, proved to be compatible with the expected behavior of the phenomenon, adequately representing the stages of acceleration, deceleration and stabilization of carbonation, identified using time series analysis.

One of the main distinguishing features of this work is the use of a robust experimental database, made up of 2313 real measurements of carbonation depth obtained over two decades of natural exposure, which guarantees high reliability for training the model. In addition, instead of using fixed average values, it was decided to insert real time series of climatic and environmental variables, which brought the predictions even closer to the behavior observed in the field. The proposed hybrid architecture, by integrating statistical models with deep neural networks, was able to capture both the temporal patterns and the non-linearities of the phenomenon, resulting in more accurate and stable forecasts. The model's reliability was also strengthened through cross-validation with external data from different Brazilian regions, increasing its potential for application in real engineering contexts.

Despite the progress made, the study has some limitations. Extrapolating the results to time horizons longer than six decades depends on the stability of future climate patterns and is subject to the uncertainty inherent in forecasting models. Since the dataset is specific to Brazilian tropical climates, direct application to other geographic zones requires recalibration. Transfer learning techniques could be explored to adapt the model across different environmental contexts. Furthermore, structural variables, such as the cover thickness and the presence of cracks, were not considered in this version of the model, although they are fundamental parameters for determining the service life of concrete structures. Future studies should consider these variables, as well as testing the application of the model to accelerated carbonation tests and different concrete compositions.

In general, the results achieved by the AVR-SARIMA-LSTM-MLP ensemble metamodel were satisfactory for a wide variety of concretes distributed in several Brazilian climate zones. The ability of the predictive metamodel based on the artificial neural network ensemble to generalize knowledge about data patterns was remarkable, proving to be a robust model that transcends local specifications and the types of materials used in its training and validation. This high generalization power suggests that this tool can be applied in several Brazilian geographic regions and in concretes with different compositions and curing conditions, contributing to the durability of concrete structures.

CRediT authorship contribution statement

Tiago Ferreira Campos Neto: Writing – review & editing, Writing – original draft, Visualization, Validation, Methodology, Investigation, Formal analysis, Data curation, Conceptualization. **Oswaldo Cascudo:** Writing – review & editing, Validation, Supervision, Resources, Project administration, Funding acquisition, Conceptualization.

Funding sources

This work was based upon a P&D Project from National Electric Energy Agency of Brazil (ANEEL) – P&D 0394-1504-2015, supported by Eletrobras Furnas with FUNAPE cooperation. The first author was supported by the University of Rio Verde (individual training leave scholarship grant number 001/2021).

Declaration of competing interest

The authors declare the following financial interests/personal relationships which may be considered as potential competing interests:Tiago Ferreira Campos Neto reports financial support provided by Eletrobras Furnas. Tiago Ferreira Campos Neto reports financial support provided by University of Rio Verde. Oswaldo Cascudo reports financial support provided by Eletrobras Furnas. Tiago Ferreira Campos Neto and Oswaldo Cascudo have patent pending to Universidade Federal de Goiás. If there are other authors, they declare that they have no known competing financial interests or personal relationships that could have appeared to influence the work reported in this paper.

Acknowledgment

The authors would like to thank the National Electric Energy Agency of Brazil (ANEEL), Eletrobras Furnas and the Brazilian governmental institutions CAPES and CNPq, which provided grants to researchers. Finally, the first author would also like to thank the University of Rio Verde (UniRV) for granting him an individual training leave scholarship.

APPENDIX A

Table A.1 lists the concretes produced and monitored by the GEDur group over 20 years of exposure to natural carbonation, including information on the composition and identification of the various samples.

Table A.1
List with identification and information on the concrete samples from the GEDur group used in the training and validation stages of the SARIMA-LSTM-MLP predictor models.

Sample	w/b ratio	Curing condition	Type of mineral addition (content)	Cement consumption (kg/m^3)	f_{ck} (MPa)	Water absorption (%)	Alternative identification
1	0.40	Wet	Reference (0 %)	552.0	25	4.43	R4W
2	0.55			368.0	20	6.04	R5W
3	0.70			274.0	15	5.65	R7W
4	0.40		Blast furnace slag (65 %)	193.2	30	4.57	BFS4W
5	0.55			128.8	25	3.82	BFS5W
6	0.70			95.9	20	5.32	BFS7W
7	0.40		Silica fume (10 %)	496.8	40	4.64	SF4W
8	0.55			331.2	30	3.16	SF5W
9	0.70			246.6	20	5.13	SF7W
10	0.40		Metakaolin (10 %)	496.8	30	5.03	M4W
11	0.55			331.2	30	4.95	M5W
12	0.70			246.6	20	5.66	M7W
13	0.40		Fly ash (25 %)	414.0	30	3.98	FA4W
14	0.55			276.0	20	4.62	FA5W
15	0.70			205.5	25	5.38	FA7W
16	0.40		Rice husk ash (10 %)	496.8	35	3.85	RHA4W
17	0.55			331.2	25	3.67	RHA5W
18	0.70			246.6	20	4.74	RHA7W
19	0.40	Dry	Reference (0 %)	552.0	25	4.43	R4D
20	0.55			368.0	20	6.04	R5D
21	0.70			274.0	15	5.65	R7D
22	0.40		Blast furnace slag (65 %)	193.2	30	4.57	BFS4D
23	0.55			128.8	25	3.82	BFS5D
24	0.70			95.9	20	5.32	BFS7D
25	0.40		Silica fume (10 %)	496.8	40	4.64	SF4D
26	0.55			331.2	30	3.16	SF5D
27	070			246.6	20	5.13	SF7D
28	0,40		Metakaolin (10 %)	496.8	30	5.03	M4D
29	0,55			331.2	30	4.95	M5D
30	0,70			246.6	20	5.66	M7D
31	0.40		Fly ash (25 %)	414.0	30	3.98	FA4D
32	0.55			276.0	20	4.62	FA5D
33	0.70			205.5	25	5.38	FA7D
34	0.40		Rice husk ash (10 %)	496.8	35	3.85	RHA4D
35	0.55			331.2	25	3.67	RHA5D
36	0.70			246.6	20	4.74	RHA7D

Table A.2 lists the concretes used to assess the generalization power of the AVR-SARIMA-LSTM-MLP ensemble predictor metamodel, including information on the composition and identification of the various samples. This list includes concretes from the research by Meira, Padaratz and Borba [85], Pauletti [86], Tasca [87] and Silveira [88].

Table A.2
List with identification and information on the concrete samples from various researchers used in the evaluation phase of the knowledge generalization power of the AVR-SARIMA-LSTM-MLP ensemble predictor metamodel.

Samples	Databases	w/b ratio	Curing condition	Type of mineral addition (content)	Cement consumption (kg/m^3)	f_{ck} (MPa)	Water absorption (%)
37	Tasca [87] and Silveira [88]	0.45	Wet	R (0 %)	394.0	55.0	1.10
38		0.45		SF (10 %)	3560	70.0	3.33
39		0.45		FA (25 %)	290.0	35.0	4.02
40		0.45		RHA (25 %)	290.0	50.0	2.96
41		0.35		R (0 %)	539.0	60.0	0.50
42		0.35		SF (10 %)	482.0	70.0	3.33
43		0.35		FA (25 %)	445.0	55.0	2.74
44		0.35		RHA (25 %)	395.0	65.0	2.48
45		0.55		R (0 %)	307.0	40.0	2.93
46		0.55		SF (10 %)	275.0	50.0	3.82
47		0.55		FA (25 %)	228.0	30.0	4.34
48		0.55		RHA (25 %)	228.0	40.0	3.44
49	Meira, Padaratz and Borba	0.50	Wet	R (0 %)	444.3	20.0	5.17
50	Júnior [85]	0.57			379.5	20.0	5.46
51		0.65			305.3	15.0	5.78
52		0.50			444.3	20.0	5.17
53		0.57			379.5	20.0	5.46
54		0.65			305.3	15.0	5.78
55		0.50			444.3	20.0	5.17
56		0.57			379.5	20.0	5.46
57		0.65			305.3	15.0	5.78
58		0.50			444.3	20.0	5.17
59		0.57			379.5	20.0	5.46
60		0.65			305.3	15.0	5.78
61	Pauletti [86]	0.40	Wet	R (0 %)	668.1	35.0	3.54
62		0.40		R (0 %)	668.1	35.0	3.54
63		0.40		R (0 %)	668.1	35.0	3.54
64		0.40		FA (40 %)	389.7	40.0	3.70
65		0.40		FA (40 %)	389.7	40.0	3.70
66		0.40		FA (40 %)	389.7	40.0	3.70
67		0.55		R (0 %)	480.7	25.0	4.76
68		0.55		R (0 %)	480.7	25.0	4.76
69		0.55		R (0 %)	480.7	25.0	4.76
70		0.55		FA (40 %)	282.6	25.0	4.66
71		0.55		FA (40 %)	282.6	25.0	4.66
72		0.55		FA (40 %)	282.6	25.0	4.66
73		0.70		R (0 %)	374.8	20.0	5.37
74		0.70		R (0 %)	374.8	20.0	5.37
75		0.70		R (0 %)	374.8	20.0	5.37
76		0.70		FA (40 %)	221.3	15.0	5.30
77		0.70		FA (40 %)	221.3	15.0	5.30
78		0.70		FA (40 %)	221.3	15.0	5.30

APPENDIX B

Figures B.1 to B.3 show the historical temperatures, relative air humidities and atmospheric CO_2 concentrations, respectively, measured in the aging environment and taken from the Goiânia weather station (INMET [69]) and the Mauna Loa Observatory (NOAA [70]).

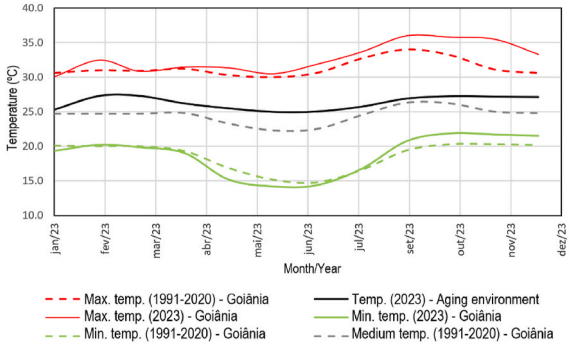

Figura B.1. Temperatures (maximum, minimum and average) collected from the weather station (last climatological normal and 2023) in Goiânia/GO and measured in the aging environment throughout 2023.

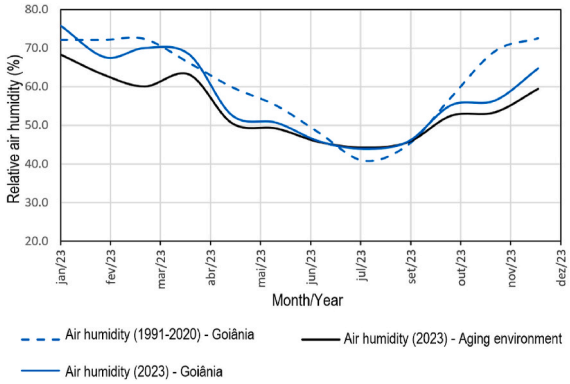

Figura B.2. Actual relative air humidities collected from the weather station (last climatological normal and 2023) in Goiânia/GO and measured in the aging environment throughout the year 2023.

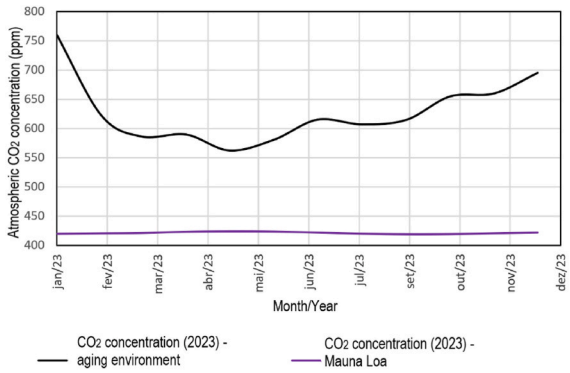

Figura B.3. Atmospheric CO_2 concentrations collected from the Mauna Loa Observatory (NOAA [70]) and measured in the aging environment throughout the year 2023.

APPENDIX C

Figure C.1 shows the results of the predictions and losses from the training and validation phases obtained by implementing the individual SARIMA-LSTM-MLP predictor models on samples 11 (M5W), 15 (FA7W), 16 (RHA4W), 19 (R4D), 24 (BFS7D) and 26 (SF5D) of the concretes from the GEDur group. The titles of the prediction results graphs show the sample number, the activation function of the output layer, the number of the training round, the batch and sequence sizes adopted and, finally, the file extension, for example, for sample 11 (M5W) the title is 11_linear_0_1_12_.h5.

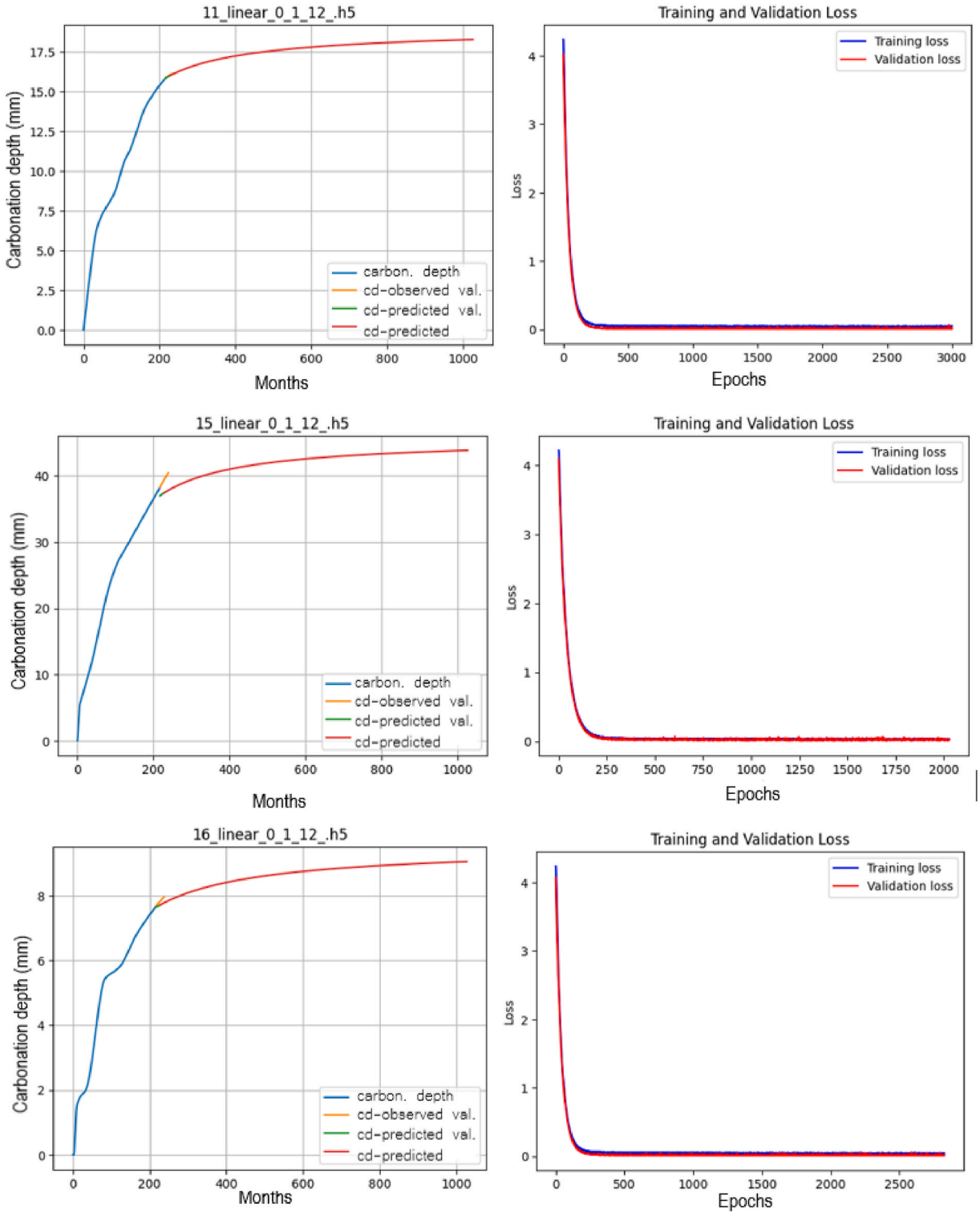

Figura C.1. Predictions of carbonation depths and training and validation losses of SARIMA-LSTM-MLP models for samples 11 (M5W), 15 (FA7W), 16 (RHA4W), 19 (R4D), 24 (BFS7D) and 26 (SF5D)

Predictions of carbonation depths and training and validation losses of SARIMA-LSTM-MLP models for samples 11 (M5W), 15 (FA7W), 16 (RHA4W), 19 (R4D), 24 (BFS7D) and 26 (SF5D).

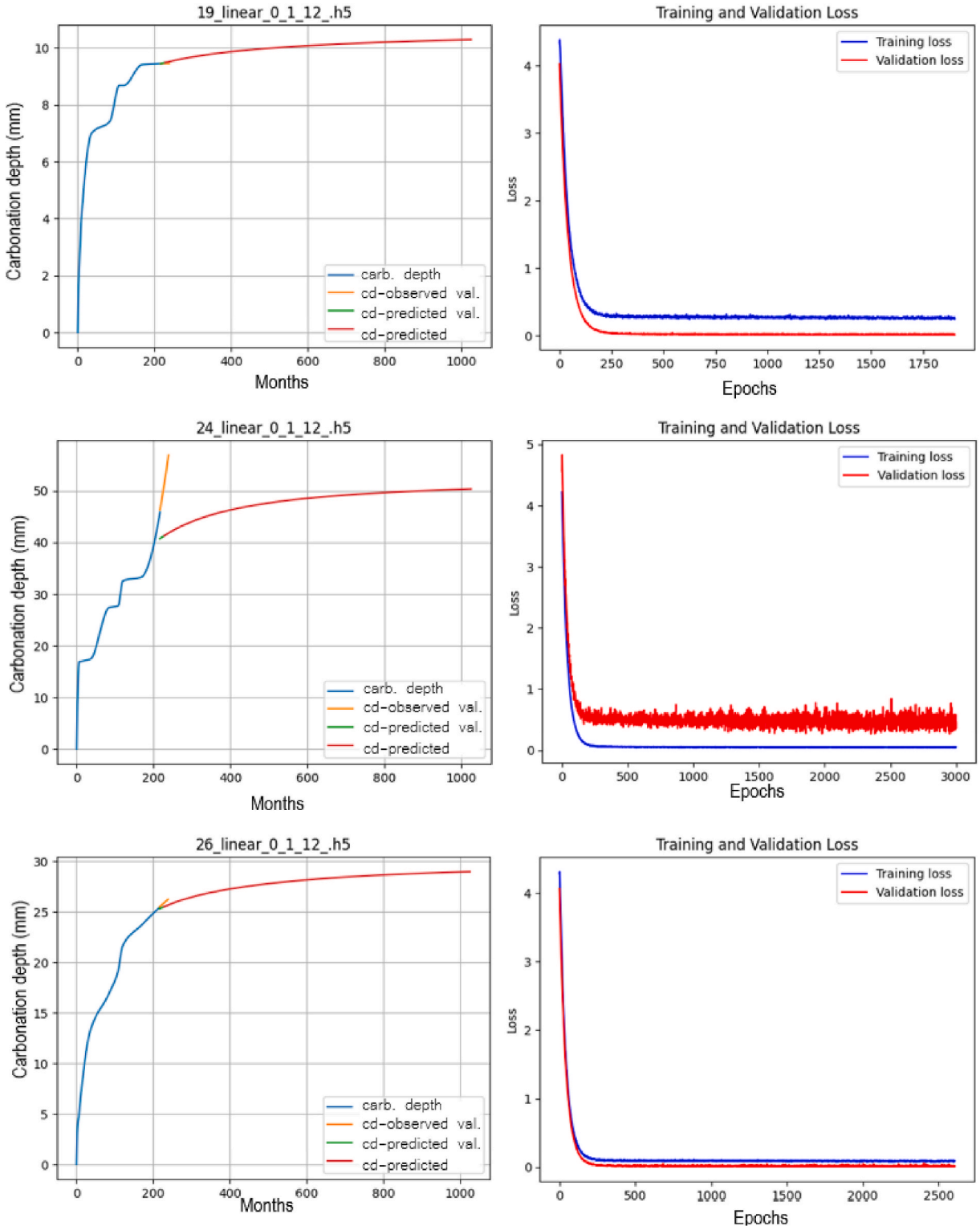

Figura C.1. (*continued*).

APPENDIX D

This appendix shows the observed and predicted carbonation curves with the AVR-SARIMA-LSTM-MLP ensemble metamodel of

concrete samples from the GEDur group databases (Figure D.1), Tasca [87] and Silveira [88] (Figure D.2), Meira, Padaratz and Borba Júnior [85] (Figure D.3) and Pauletti [86] (Figure D.4). The title of each graph notes the sample number, the term function, the round number, the batch and the sequence sizes adopted as part of the artificial neural networks hyperparameters and, finally, the file extension, for example, for sample 1 (R4W) the title is 1_function_0_1_12_.h5.

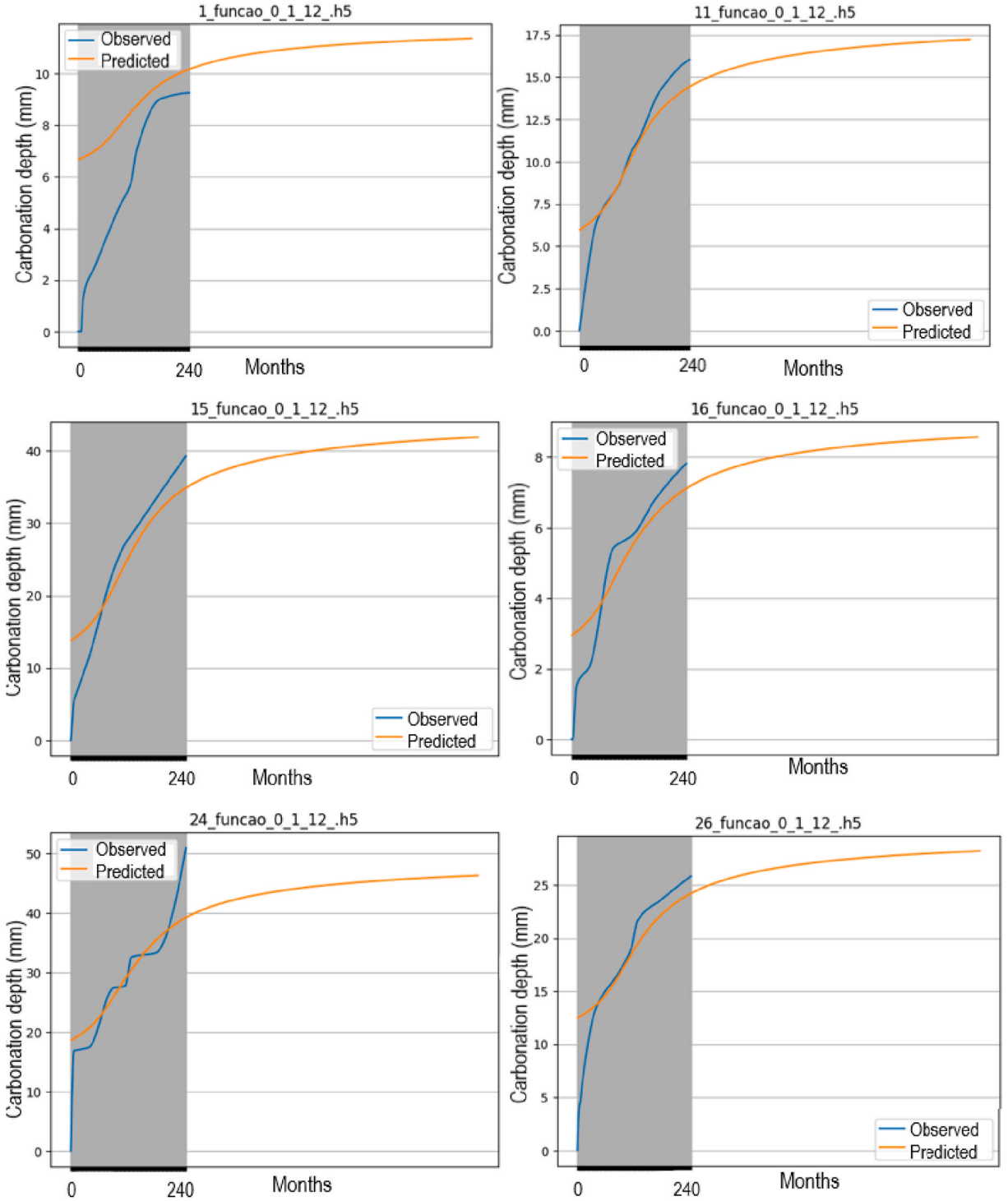

Figura D.1. Results of the actual/observed (blue lines with gray highlight) and predicted (orange lines) carbonation depth curves by the AVR-SARIMA-LSTM-MLP ensemble metamodel up to 806 months (approximately 67 years) for samples 1 (R4W), 11 (M5W), 15 (FA7W), 16 (RHA4W), 24 (BFS7D) and 26 (SF5D) from the GEDur group.

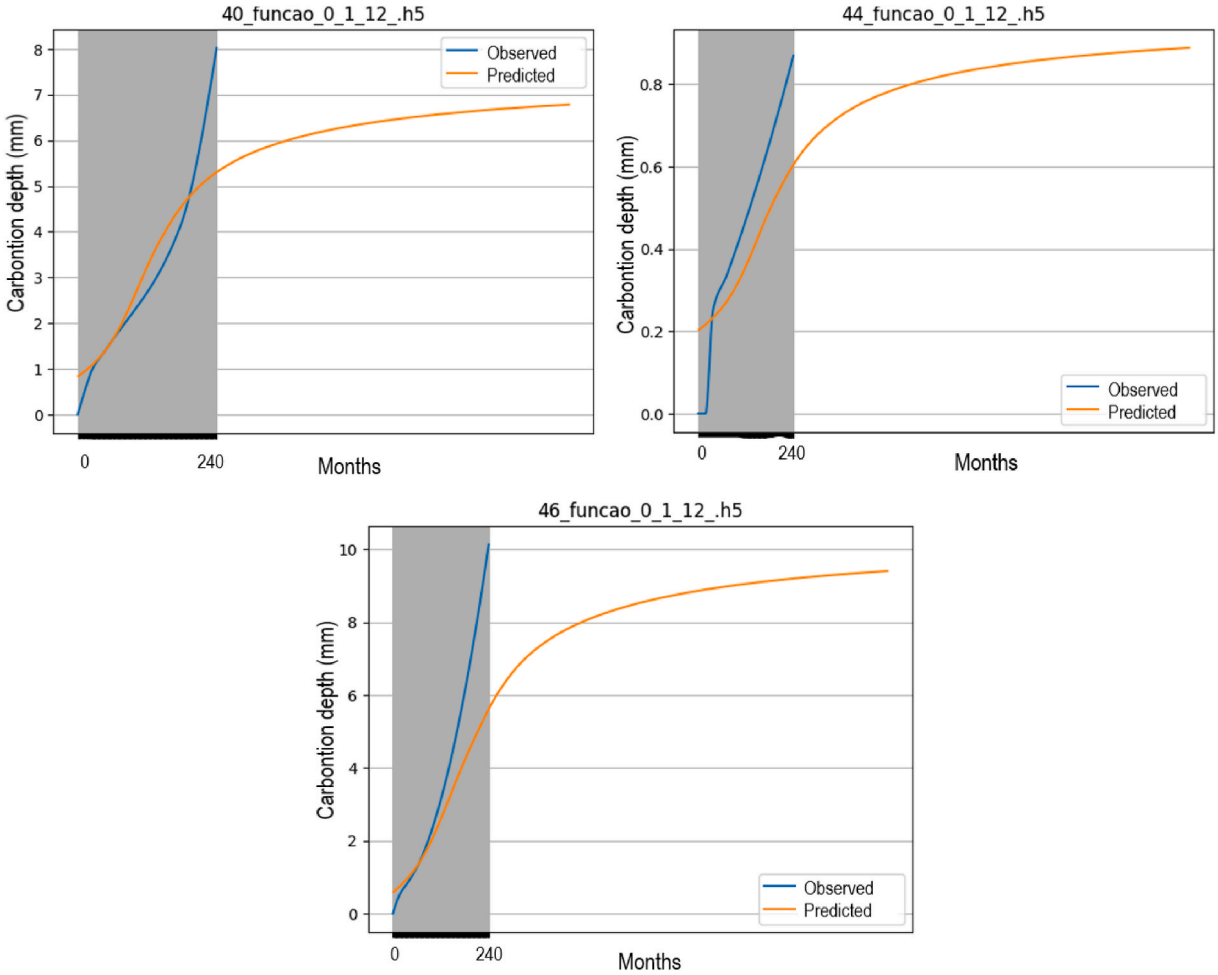

Figura D.2. Results of the actual/observed (blue lines with gray highlight) and predicted (orange lines) carbonation depth curves by the AVR-SARIMA-LSTM-MLP ensemble metamodel up to 806 months (approximately 67 years) for samples 40, 44 and 46 from Tasca [87] and Silveira [88].

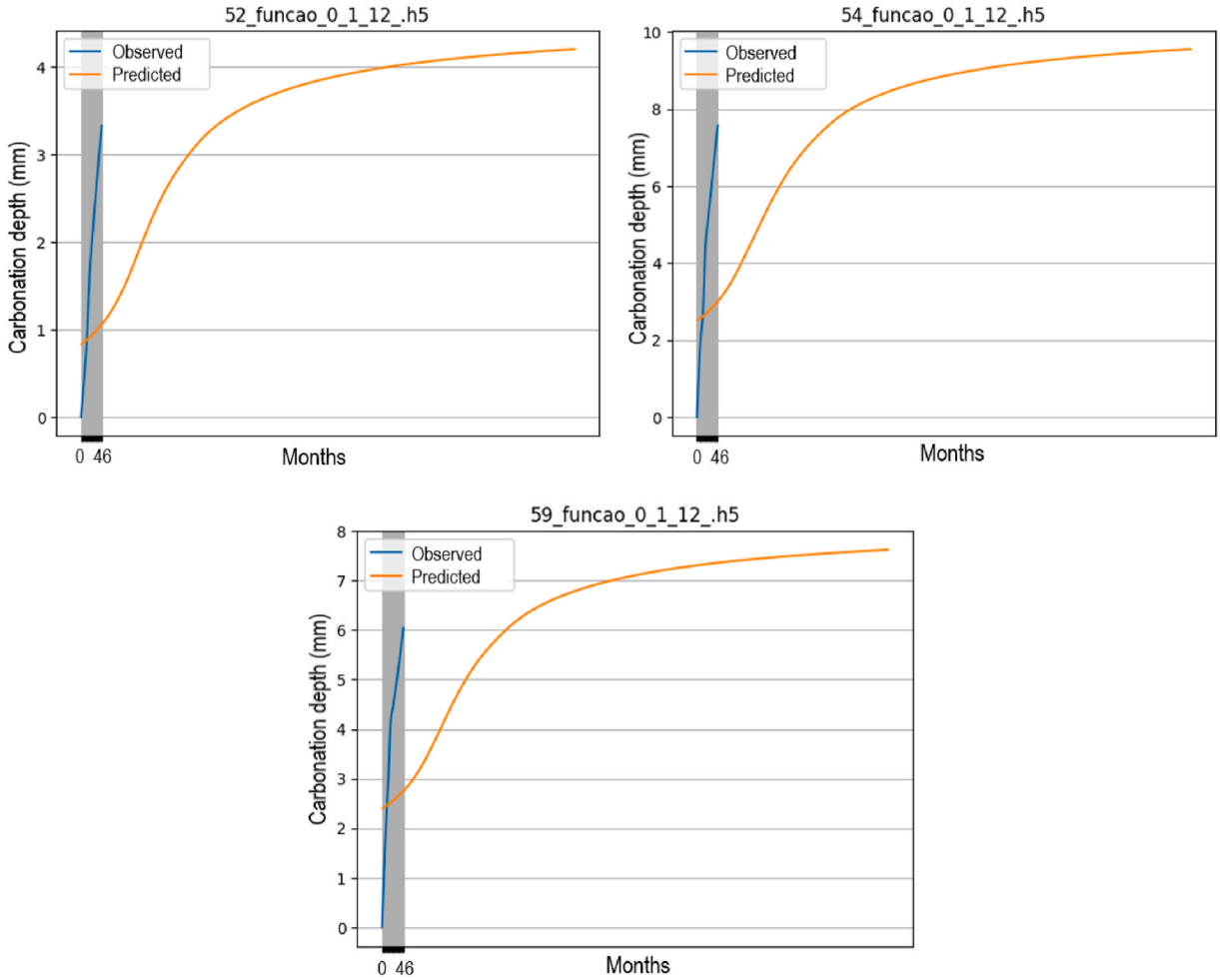

Figura D.3. Results of the actual/observed (blue lines with gray highlight) and predicted (orange lines) carbonation depth curves by the AVR-SARIMA-LSTM-MLP ensemble metamodel up to 806 months (approximately 67 years) for samples 52, 54 and 59 from Meira, Padaratz and Borba Júnior [85].

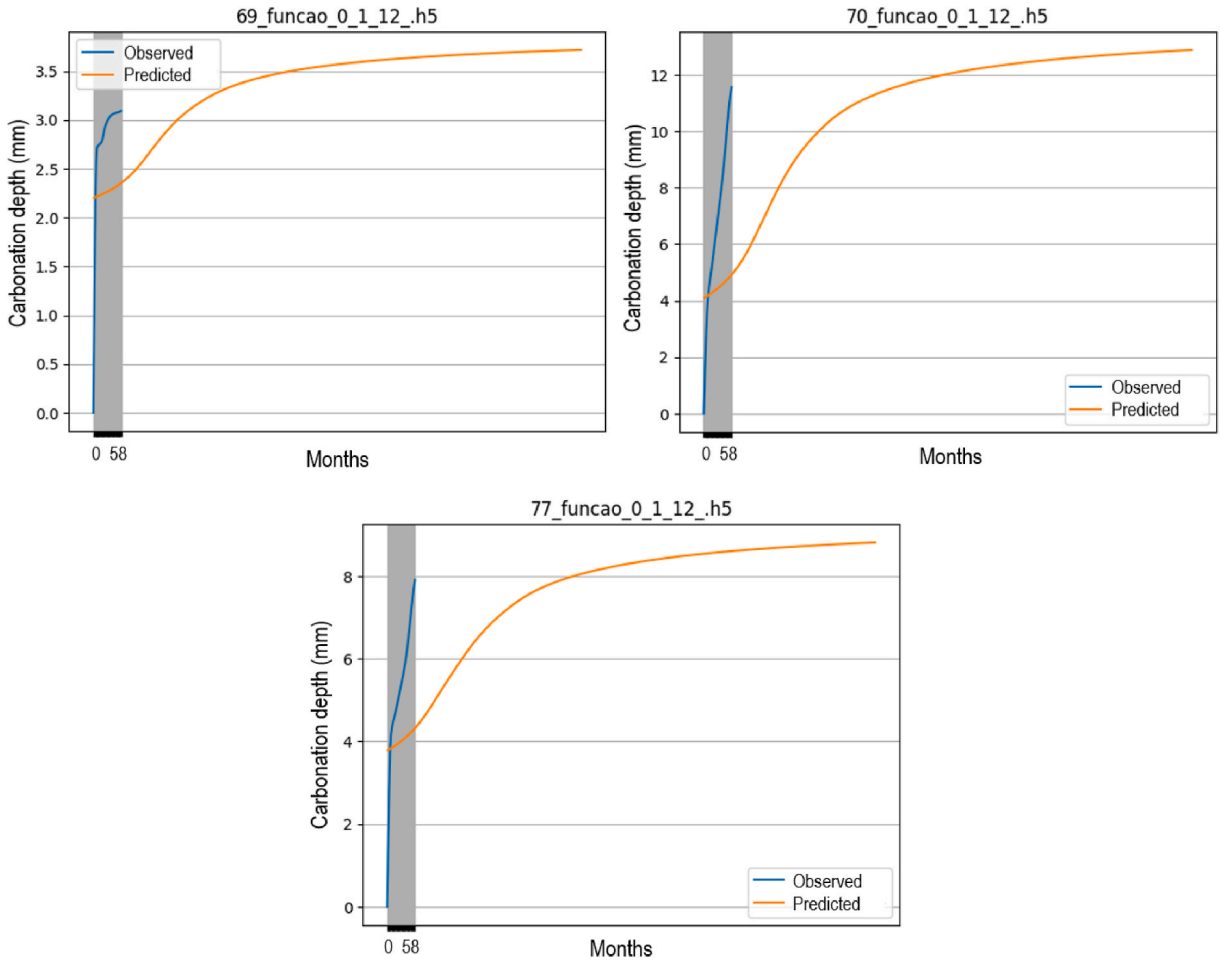

Figura D.4. Results of the actual/observed (blue lines with gray highlight) and predicted (orange lines) carbonation depth curves by the AVR-SARIMA-LSTM-MLP ensemble metamodel up to 806 months (approximately 67 years) for samples 69, 70 and 77 from Pauletti [86].

Data availability

Data will be made available on request.

References

[1] B. Youn, A study on application of deep learning algorithm for the prediction of carbonation rate coeficiente of the underground concrete structures, Fukuoka, 2021. Department of Civil and Structural Engineering, Kyushu University, Fukuoka, 2021. Dissertation (Doctoral in Engineering).
[2] O. Cascudo, H. Carasek, Carbonatação no concreto, in: G.C. ISAIA (Ed.), Concreto: Ciência e Tecnologia, vol. 3, IBRACON, São Paulo, 2022.
[3] M.H.F. Medeiros, J.J.O. Andrade, P. Helene, Durabilidade e vida útil das estruturas de concreto, in: G.C. ISAIA (Ed.), Concreto: Ciência e Tecnologia, vol. 3, IBRACON, São Paulo, 2022.
[4] T.F. Campos Neto, A dinâmica temporal da carbonatação em estruturas de concreto: Investigação com análises de séries temporais e previsão com redes neurais artificiais, Goiânia, Dissertation (Doctoral in Civil Engineering), School of Civil and Environmental Engineering, Federal University of Goiás, Goiânia, 2024, 2024.
[5] M.P. Kwlakowski, Contribuição ao estudo da carbonatação em concretos e argamassas compostos com adição de sílica ativa, in: Porto Alegre (Ed.), School of Civil Engineering, Federal University of Rio Grande do Sul, Porto Alegre, 2002, 2002. Dissertation (Doctoral in Civil Engineering).
[6] P.F. Pires, Estudo da carbonatação avançada em concretos contendo adições minerais, Goiânia, 2016. Thesis (Masters in Civil Engineering), School of Civil and Environmental Engineering, Federal University of Goiás, Goiânia, 2016.
[7] C. Pauletti, E. Possan, D.C.C. Dal Molin, Carbonatação acelerada: Estado da arte das pesquisas no Brasil, Ambiente Construído 7 (4) (2007), https://doi.org/10.1016/j.conbuildmat.2015.06.007.
[8] H. Cui, W. Tang, W. Liu, Z. Dong, F. Xing, Experimental study on effects of CO2 concentrations on concrete carbonation and diffusion mechanisms, Constr. Build. Mater. 93 (2015).
[9] S.O. Ekolu, A review on effects of curing, sheltering, and CO2 concentration upon natural carbonation of concrete, Constr. Build. Mater. 127 (2016), https://doi.org/10.1016/j.conbuildmat.2016.09.056.

[10] Y. Chen, P. Liu, Z. Yu, Effects of environmental factors on concrete carbonation depth and compressive strength, Materials 11 (11) (2018), https://doi.org/10.3390/ma11112167.
[11] T.J. Silva, Mecanismos de transporte de massa no concreto, in: G.C. ISAIA (Ed.), Concreto: Ciência e Tecnologia, vol. 3, 2022. São Paulo: IBRACON.
[12] F. Lollini, E. Redaelli, Carbonation of blended cement concretes after 12 years of natural exposure, Constr. Build. Mater. 276 (2021), https://doi.org/10.1016/j.conbuildmat.2020.122122.
[13] E. Gruyaert, P.V. Heede, N.D. Belie, Carbonation of slag concrete: effect of the cement replacement level and curing on the carbonation coefficient – effect of carbonation on the pore structure, Cement Concr. Res. 35 (2013), https://doi.org/10.1016/j.cemconcomp.2012.08.024.
[14] A. Leemann, F. Moro, Carbonation of concrete: the role of CO_2 concentration, relative humidity and CO_2 buffer capacity, Mater. Struct. 50 (2017), https://doi.org/10.1617/s11527-016-0917-2.
[15] P. Liu, Y. Chen, Z. Yu, Effects of temperature, relative humidity and carbon dioxide concentration on concrete carbonation, Mag. Concr. Res. 72 (18) (2020), https://doi.org/10.1680/jmacr.18.00496.
[16] H.G. Smolczyk, Written discussion, in: V. Tokyo (Ed.), The International Symposium on the Chemistry of Cement, 1969. **Proceedings** [...] Tokyo, 1969, Part III, v. II/4.
[17] L. Sentler, Stochastic characterization of carbonation of concrete. International Conference on Durability of Building Materials and Components, 1984, 3, Espoo, 1984. Proceedings [...] Espoo.
[18] V.G. Papadakis, C.V. Vayenas, M.N. Fardis, Fundamental modeling and experimental investigation of concrete carbonation, ACI Mater. J. 88 (4) (1991), https://doi.org/10.14359/1863.
[19] C. Bob, E. Afana, On-site assessment of concrete carbonation, in: International Conference Failure of Concrete Structures, Bratislava, RILEM, Bratislava, 1993, 1993. Proceedings.
[20] P.R.L. Helene, Vida útil das estruturas de concreto, in: Congresso Iberoamericano de Patologia das Construções, vol. 4, Porto Alegre, 1997. **Anais** [...] Porto Alegre, 1997.
[21] C. Andrade, Calculation of initiation and propagation periods of service life of reinforcements by using the electrical resistivity. International RILEM Symposium on Concrete Science and Engineering: A Tribute to Amon Bentur, 2004. Paris, 2004. **Proceedings** [...] Paris: RILEM.
[22] E. Possan, Modelagem da carbonatação e precisão de vida útil de estruturas de concreto em ambiente urbano, Porto Alegre. Dissertation (Doctoral in Civil Engineering), Department of Civil Engineering, Federal University of Rio Grande do Sul, Porto Alegre, 2010, 2010.
[23] FÉDERATION INTERNATIONALE DU BÉTON, Fib (CEB-FIP) Model Code for Concrete Structures 2020, Lausanne: Ernst & Sohn, 2024.
[24] X. Zha, M. Yu, J. Ye, G. Feng, Numerical modeling of supercritical carbonation process in cement-based materials, Cement Concr. Res. 72 (2015), https://doi.org/10.1016/j.cemconres.2015.02.017.
[25] S.O. Ekolu, Model for practical prediction of natural carbonation in reinforced concrete: Part 1-formulation, Cement Concr. Compos. 86 (2018), https://doi.org/10.1016/j.cemconcomp.2017.10.006.
[26] K. Tuutti, Corrosion of steel in concrete. Division of Building Materials, Swedish Cement and Concrete Research Institute, Stockholm, 1982. Stockholm, 1982. Dissertation (Doctoral in Civil Engineering).
[27] B. Liang, F. Sun, Prediction of concrete material based on PSO algorithm, J. Build. Struct. 27 (2006).
[28] N. Ukrainczyk, V. Ukrainczyk, A neural network method for analyzing concrete durability, Mag. Concr. Res. 60 (2008), https://doi.org/10.1680/macr.2007.00016.
[29] E.F. Félix, E. Possan, Modeling the carbonation front of concrete structures in the marine environment through ANN, IEEE Latin America Transactions 16 (6) (2018), https://doi.org/10.1109/TLA.2018.8444398.
[30] S. Moghaddas, M. Nekoei, E.G. Mohammadi, M. Nehdi, M. Arashpour, Modeling carbonation depth of recycled aggregate concrete using novel automatic regression technique, J. Clean. Prod. 371 (2022), https://doi.org/10.1016/j.jclepro.2022.133522.
[31] Y. Wei, P. Chen, S. Cao, H. Wang, Y. Liu, Z. Wang, W. Zhao, Prediction of carbonation depth for concrete containing mineral admixtures based on machine learning, Arabian J. Sci. Eng. 48 (2023), https://doi.org/10.1007/s13369-023-07645-8.
[32] S. Kwon, H. Song, Analysis of carbonation behavior in concrete using neural network algorithm and carbonation modeling, Cement Concr. Res. 40 (1) (2010), https://doi.org/10.1016/j.cemconres.2009.08.022.
[33] D. Luo, D. Niu, Z. Dong, Application of neural network for concrete carbonation depth prediction, in: International Conference on the Durability of Concrete Structures (ICDCS), 4, 2014, Indiana, 2014. Proceedings [...] Indiana.
[34] B. Boukhatem, A. Tagnit-Hamou, M. Chekired, M. Ghrici, Towards a service life prediction system of concrete structures based on a neural-computing approach, in: RILEM International Conference on Cementitious Materials and Alternative Binders for Sustainable Concrete (ICCM), vol. 10, 2017. Montreal, 2017. Procedings [...], Montreal.
[35] Y. Kellouche, B. Boukhatem, M. Ghrici, A. Tagnit-Hamou, Exploring the major factors affecting fly-ash concrete carbonation using artificial neural network, Neural Comput. Appl. 31 (2017), https://doi.org/10.1007/s00521-017-3052-2.
[36] W.Z. Taffese, E. Sistonen, Machine learning for durability and service-life assessment of reinforced concrete structures: recent advances and future directions, Autom. ConStruct. 77 (2017), https://doi.org/10.1016/j.autcon.2017.01.016.
[37] S. Paul, B. Panda, Y. Huang, A. Garg, X. Peng, An empirical model design for evaluation and estimation of carbonation depth in concrete, Measurement 124 (2018), https://doi.org/10.1016/j.measurement.2018.04.033.
[38] S. Verma, J. Kujur, Water permeability and carbonation modelling of different variants of concrete using ANN, Malaysian Construction Research Journal 26 (3) (2018).
[39] E.F. Félix, E. Possan, R. Carrazedo, Analysis of training parameters in the ANN learning process to mapping the concrete carbonation depth, Journal of Building Pathology and Rehabilitation 4 (1) (2019), https://doi.org/10.1007/s41024-019-0054-8.
[40] W. Gao, D. Chen, Prediction model of service life for tunnel structures in carbonation environments by genetic programming, Geomechanics and Engineering 18 (4) (2019), https://doi.org/10.12989/gae.2019.18.4.373.
[41] P. Akpinar, I.D. Uwanuakwa, Investigation of the parameters influencing progress of concrete carbonation depth by using artificial neural networks, Mater. Construcción 70 (337) (2020), https://doi.org/10.3989/mc.2020.02019.
[42] H. Lee, H.S. Lee, P. Suraneni, Evaluation of carbonation progress using AIJ model, FEM analysis, and machine learning algorithms, Constr. Build. Mater. 259 (2020), https://doi.org/10.1016/j.conbuildmat.2020.119703.
[43] I. Uwanuakwa, P. Akpinar, Investigations on the influence of variations in hidden neurons and training data percentage on the efficiency of concrete carbonation depth prediction with ann,, in: International Conference on Theory and Application of Soft Computing, Computing with Words and Perceptions (ICSCCW), vol. 10, 2019. Prague, 2019. Proceedings [...] Prague.
[44] E.F. Félix, R. Carrazedo, E. Possan, Carbonation model for fly ash concrete based on artificial neural network: development and parametric analysis, Constr. Build. Mater. 266 (2021), https://doi.org/10.1016/j.conbuildmat.2020.121050.
[45] Y. Kellouche, M. Ghrici, B. Boukhatem, Service life prediction of fly ash concrete using an artificial neural network, Front. Struct. Civ. Eng. 15 (2021), https://doi.org/10.1007/s11709-021-0717-9.
[46] Y. Kellouche, B. Boukhatem, M. Ghrici, R. Rebouh, A. Zidol, Neural network model for predicting the carbonation depth of slag concrete, Asian Journal of Civil Engineering 22 (7) (2021), https://doi.org/10.1007/s42107-021-00390-z.
[47] Y.X. Tang, Y.H. Lee, M. Amran, R. Fediuk, N. Vatin, A.B.H. Kueh, Y.Y. Lee, Artificial neural network-forecasted compression strength of alkaline-activated slag concretes, Sustainability 14 (2022), https://doi.org/10.3390/su14095214.
[48] I. Yakub, A.B.H. Kueh, E.A.P. De La O, M.R. Rahman, M.H. Barawi, M.O. Abdullah, M. Amran, R. Fediuk, N.I. Vatin, Employing an artificial neural network in correlating a hydrogen-selective catalytic reduction performance with crystallite sizes of a biomass-derived bimetallic catalyst, Catalysts 12 (2022), https://doi.org/10.3390/catal12070779.

[49] O.T. Biala, A comparative study of CatBoost and artificial neural networks in enhancing trip generation modelling for Ilorin City, Journal of Civil Engineering, Science and Technology 15 (2024), https://doi.org/10.33736/jcest.6196.2024.
[50] K. Liu, M.S. Alam, J. Zhu, J. Zheng, L. Chi, Prediction of carbonation depth for recycled aggregate concrete using ANN hybridized with swarm intelligence algorithms, Constr. Build. Mater. 301 (2021), https://doi.org/10.1016/j.conbuildmat.2021.124382.
[51] I. Nunez, M.L. Nehdi, Machine learning prediction of carbonation depth in recycled aggregate concrete incorporating SCMs, Constr. Build. Mater. 287 (2021), https://doi.org/10.1016/j.conbuildmat.2021.123027.
[52] R. Biswas, E. Li, N. Zhang, S. Kumar, B. Rai, J. Zhou, Development of hybrid models using metaheuristic optimization techniques to predict the carbonation depth of fly ash concrete, Constr. Build. Mater. 346 (2022), https://doi.org/10.1016/j.conbuildmat.2022.128483.
[53] K. Duan, S. Cao, Data-driven parameter selection and modeling for concrete carbonation, Materials 15 (9) (2022), https://doi.org/10.3390/ma15093351.
[54] H. Hafez, A. Teirelbar, R. Kurda, N. Tosic, A. Fuente, Pre-bcc: a novel integrated machine learning framework for predicting mechanical and durability properties of blended cement concrete, Constr. Build. Mater. 352 (2022), https://doi.org/10.1016/j.conbuildmat.2022.129019.
[55] S. Hussain, D. Bhunia, S. Singh, J. Yadav, A study on the carbonation of binary and ternary blended cement mortar and concrete, Journal of Structural Integrity and Maintenance 7 (1) (2022), https://doi.org/10.1080/24705314.2021.1971892.
[56] T.H. Kwon, J. Kim, K.T. Park, K.S. Jung, Long short-term memory-based methodology for predicting carbonation models of reinforced concrete slab bridges: case study in South Korea, Appl. Sci. 12 (2022), https://doi.org/10.3390/app122312470.
[57] S.N. Londhe, P.S. Kulkarni, P.R. Dixit, A. Silva, R. Neves, J. Brito, Tree based approaches for predicting concrete carbonation coefficient, Applied Sciences-Basel 12 (8) (2022), https://doi.org/10.3390/app12083874.
[58] H. Naseri, H. Jahanbakhsh, K. Khezri, A.J. Shirzadi, Toward sustainability in optimizing the fly ash concrete mixture ingredients by introducing a new prediction algorithm, Environ. Dev. Sustain. 24 (2) (2022), https://doi.org/10.1007/s10668-021-01554-2.
[59] V. Tran, H. Mai, Q. To, M. Nguyen, Machine learning approach in investigating carbonation depth of concrete containing fly ash, Struct. Concr. 24 (2) (2022), https://doi.org/10.1002/suco.202200269.
[60] J. Forsdyke, B. Zviazhynski, J. Lees, G. Conduit, Probabilistic selection and design of concrete using machine learning, Data-Centric Engineering 4 (2023), https://doi.org/10.48550/arXiv.2304.11226.
[61] M. Kumar, M. Kumar, S. Singh, S. Kim, A. Anand, S. Pandey, S. Hasnain, A. Ragab, A. Deifalla, A hybrid model based on convolution neural network and long short-term memory for qualitative assessment of permeable and porous concrete, Case Stud. Constr. Mater. 19 (2023), https://doi.org/10.1016/j.cscm.2023.e02254.
[62] A. Majlesi, H.K. Koodiani, O.T. Rincon, A. Montoya, V. Millano, A.A.T. Acosta, B.C.R. Troconis, Artificial neural network model to estimate the long-term carbonation depth of concrete exposed to natural environments, J. Build. Eng. 74 (2023), https://doi.org/10.1016/j.jobe.2023.106545.
[63] P. Miao, H. Yokota, Y. Zhang, Deterioration prediction of existing concrete bridges using a LSTM recurrent neural network, Structure and Infrastructure Engineering 19 (2023), https://doi.org/10.1080/15732479.2021.1951778.
[64] A. Géron, Mãos à obra: Aprendizado de máquina com Scikit-Learn, vol. 2, Keras & TensorFlow, Rio de Janeiro, 2021. Alta Books.
[65] A. Mohammed, R.A. Kora, A comprehensive review on ensemble deep learning: opportunities and challenges, J. King Saud Univ. Comput. Inf. Sci. 35 (2) (2023), https://doi.org/10.1016/j.jksuci.2023.01.014.
[66] W.Z. Taffese, E. Sistonen, Significance of chloride penetration controlling parameters in concrete: ensemble methods, Constr. Build. Mater. 139 (2017), https://doi.org/10.1016/j.conbuildmat.2017.02.014.
[67] A. Castro, Influência das adições minerais na durabilidade do concreto sujeito à carbonatação, Goiânia, 2003. Thesis (Masters in Civil Engineering), School of Civil and Environmental Engineering, Federal University of Goiás, Goiânia, 2003.
[68] ASSOCIAÇÃO BRASILEIRA DE NORMAS TÉCNICAS (ABNT), NBR 6118: Projeto de estruturas de concreto – Procedimento, Rio de Janeiro, 2024.
[69] INSTITUTO NACIONAL DE METEOROLOGIA (INMET), Banco de dados meteorológicos, Ministério da Agricultura e Pecuária, 2023. Available at: https://bdmep.inmet.gov.br/. (Accessed 22 April 2023).
[70] THE NATIONAL OCEANIC AND ATMOSPHERIC ADMINISTRATION (NOAA), Trends in atmospheric carbon dioxide, Global Monitoring Laboratory (2023). Available at: https://gml.noaa.gov/ccgg/trends/gr.html. (Accessed 12 March 2023).
[71] AMERICAN SOCIETY FOR TESTING MATERIALS, ASTM E 178-21: Standard Practice for Dealing with Outlying Observations, 2021. West Conshohocken.
[72] P. Dangla, W. Dridi, Rebar corrosion in carbonated concrete exposed to variable humidity conditions. Interpretation of Tuutti's curve, Corros. Sci. 51 (8) (2009), https://doi.org/10.1016/j.corsci.2009.04.029.
[73] I. Monteiro, F.A. Branco, J. Brito, R. Neves, Statistical analysis of the carbonation coefficient in open air concrete structures, Constr. Build. Mater. 29 (2012), https://doi.org/10.1016/j.conbuildmat.2011.10.028.
[74] M.B. Ferreira, A. Castro, O. Cascudo, H. Carasek, Avaliação da carbonatação natural ao longo do tempo de concretos com diferentes adições minerais, Congresso Brasileiro do Concreto 54 (2012). Maceió. Anais [...] São Paulo: IBRACON, 2012. v. 1.
[75] O. Cascudo, P. Pires, H. Carasek, A. Castro, A. Lopes, Evaluation of the pore solution of cocnretes with mineral additions subjected to 14 years of natural carbonation, Cement Concr. Compos. 115 (2021), https://doi.org/10.1016/j.cemconcomp.2020.103858.
[76] T.F. Campos Neto, O. Cascudo, Imputação de dados ausentes em séries temporais de carbonatação dos concretos, Ambiente Construído 24 (2024) e136386, https://doi.org/10.1590/s1678-86212024000100748.
[77] T.D. Roy, K.K. Das, Modelling of mean temperature of four stations in Assam, Int. J. Adv. Res. 4 (2016), https://doi.org/10.21474/IJAR01/2403.
[78] S. Ray, S.S. Das, P. Mishra, A.M.G. Al Khatib, Time series SARIMA modelling and forecasting of monthly rainfall and temperature in the south asian countries, Earth Systems and Environment 5 (2021), https://doi.org/10.1007/s41748-021-00205-w.
[79] THE INTERGOVERNMENTAL PANEL ON CLIMATE CHANGE (IPCC), Sixth Assessment Report (AR6 Climate Change 2022) (2023). Available at: https://www.ipcc.ch/assessment-report/ar6/. (Accessed 22 April 2023).
[80] C.J. Willmott, S.G. Ackleson, R.E. Davis, J.J. Feddema, K.M. Klink, D.R. Legates, J. O'Donnell, C.M. Rowe, Statistics for the evaluation and comparison of models, J. Geophys. Res. 90 (C5) (1985), https://doi.org/10.1029/JC090iC05p08995.
[81] A.P. Camargo, P.C. Sentelhas, Avaliação do desempenho de diferentes métodos de estimativa da evapotranspiração potential no Estado de São Paulo, Brasil, Revista Brasileira de Agrometeorologia 5 (1) (1997).
[82] L.K. Hansen, P. Salamon, Neural Network Ensembles, IEEE Transactions on Pattern Analysis and Machine Learning 12 (1990) 10, https://doi.org/10.1109/34.58871.
[83] G. Brown, J. Wyatt, R. Harris, X. Yao, Diversity creation methods: a survey and categorization, Inf. Fusion 6 (1) (2004), https://doi.org/10.1016/j.inffus.2004.04.004.
[84] Y. Liu, C. Zhao, Y. Huang, A combined model for multivariate time series forecasting based on MLP-feedforward attention-LSTM, IEEE Acess 10 (2022), https://doi.org/10.1109/ACCESS.2022.3192430.
[85] G.R. Meira, I.J. Padaratz, J.C. Borba Júnior, Carbonatação natural de concretos: Resultados de cerca de quatro anos de monitoramento, in: Encontro Nacional de Tecnologia no Ambiente Construído, XI, 2006, 2006. Florianópolis. Anais [...] Florianópolis.
[86] C. Pauletti, Estimativa da carbonatação natural de materiais cimentícios a partir de ensaios acelerados e de modelos de predição, Porto Alegre. Dissertation (Doctoral in Civil Engineering), Department of Civil Engineering, Federal University of Rio Grande do Sul, Porto Alegre, 2009, 2009.
[87] M. Tasca, Estudo da carbonatação natural de concretos com pozolanas: Monitoramento em longo prazo e análise da microestrutura, Santa Maria, Department of Civil and Environmental Engineering, Federal University of Santa Maria, Santa Maria, 2012, 2012. Thesis (Masters in Civil Engineering).
[88] R.G. Silveira, Estudo de concretos com pozolanas submetidos à carbonatação natural em ensaios acelerado e natural monitorado por 20 anos, Santa Maria, 2019. Dissertation (Doctoral in Civil Engineering), Department of Civil Engineering, Federal University of Santa Maria, Santa Maria, 2019.
[89] M.O. Vaghetti, Efeitos da cinza volante com cinza de casca de arroz ou sílica ativa sobre a carbonatação do concreto de cimento Portland, Santa Maria, Department of Civil and Environmental Engineering, Federal University of Santa Maria, Santa Maria, 1999, 1999. Thesis (Masters in Civil Engineering).

[90] E. Possan, J.J.O. Andrade, D.C.C. Dal Molin, J.L.D. Ribeiro, Model to estimate concrete carbonation depth and service life prediction, in: V.P. FREITAS, A. COSTA, J.M.P.Q. DELGADO (Eds.), Hygrothermal Behaviour and Building Pathologies, **Building Pathology and Rehabilitation**, vol. 14, Springer, California, 2021.
[91] C. Andrade, Novas diretrizes do model code 2020, in: International Seminar on Performance and Durability of Concrete Structures (DURAR), V, Universidade Federal de Goiás, Goiânia, 2023.
[92] V.T. Ngala, C.L. Page, Effect of carbonation on pore structure and diffusional properties of hydrated cement pastes, Cement Concr. Res. 27 (7) (1997), https://doi.org/10.1016/S0008-8846(97)00102-6.
[93] A.R. Martins, Efeito da cura térmica e de cimentos com escória granulada de alto-forno na durabilidade do concreto de cobrimento. Dissertação (Mestrado em Engenharia Civil) – Faculdade de Engenharia Civil, Universidade Estadual de Campinas, Campinas, 2001. Campinas, 2001.